Institut für Physik und Astronomie der Universität Potsdam
Professur für Statistische Physik und Chaostheorie

Complex Regimes of Synchronization:
Modeling and Analysis

Dissertation

zur Erlangung des akademischen Grades
"doctor rerum naturalium"
(Dr. rer. nat.)
in der Wissenschaftsdisziplin "Theoretische Physik"

eingereicht an der
Mathematisch-Naturwissenschaftlichen Fakultät
der Universität Potsdam
von

Azamat Yeldesbay

am
30 September 2014
betreut durch
apl. Prof. Dr. Michael Rosenblum

Abstract

Synchronization is a fundamental phenomenon in nature. It can be considered as a general property of self-sustained oscillators to adjust their rhythm in the presence of an interaction.

In this work we investigate complex regimes of synchronization phenomena by means of theoretical analysis, numerical modeling, as well as practical analysis of experimental data.

As a subject of our investigation we consider chimera state, where due to spontaneous symmetry-breaking of an initially homogeneous oscillators lattice split the system into two parts with different dynamics. Chimera state as a new synchronization phenomenon was first found in non-locally coupled oscillators system, and has attracted a lot of attention in the last decade. However, the recent studies indicate that this state is also possible in globally coupled systems. In the first part of this work, we show under which conditions the chimera-like state appears in a system of globally coupled identical oscillators with intrinsic delayed feedback. The results of the research explain how initially monostable oscillators became effectivly bistable in the presence of the coupling and create a mean field that sustain the coexistence of synchronized and desynchronized states. Also we discuss other examples, where chimera-like state appears due to frequency dependence of the phase shift in the bistable system.

In the second part, we make further investigation of this topic by modeling influence of an external periodic force to an oscillator with intrinsic delayed feedback. We made stability analysis of the synchronized state and constructed Arnold tongues. The results explain formation of the chimera-like state and hysteric behavior of the synchronization area. Also, we consider two sets of parameters of the oscillator with symmetric and asymmetric Arnold tongues, that correspond to mono- and bi-stable regimes of the oscillator.

In the third part, we demonstrate the results of the work, which was done in collaboration with our colleagues from Psychology Department of University of Potsdam. The project aimed to study the effect of the cardiac rhythm on human perception of time using synchronization analysis. From our part, we made a statistical analysis of the data obtained from the conducted experiment on free time interval reproduction task. We examined how ones heartbeat influences the time perception and searched for possible phase synchronization between heartbeat cycles and time reproduction responses. The findings support the prediction that cardiac cycles can serve as input signals, and is used for reproduction of time intervals in the range of several seconds.

Allgemeinverständliche Zusammenfassung

Synchronisation ist ein fundamentales Naturphänomen. Es ist die grundlegende Eigenschaft sich selbsterhaltender Oszillatoren, in Gegenwart einer Wechselwirkung, danach zu streben, ihre Rhythmen anzupassen.

In dieser Arbeit betrachten wir komplexe Synchronisationszustände sowohl mit Hilfe analytischer Methoden als auch durch numerische Simulation und in experimentellen Daten.

Unser Untersuchungsobjekt sind die sogenannten Chimera Zustände, in welchen sich Ensemble von gekoppelten, identischen Oszillatoren auf Grund eines Symmetriebruches spontan in Gruppen mit unterschiedlicher Dynamik aufteilen. Die Entdeckung von Chimeras in zunächst nichtlokal gekoppelten Systemen hat in den letzten zehn Jahren ein großes Interesse an neuartigen Synchronisationsphänomenen geweckt. Neueste Forschungsergebnisse belegen, dass diese Zustände unter bestimmten Bedingungen auch in global gekoppelten Systemen existieren können. Solche Bedingungen werden im ersten Teil der Arbeit in Ensemblen global gekoppelter Oszillatoren mit zusätzlicher, zeitverzögerter Selbstkopplung untersucht. Wir zeigen, wie zunächst monostabile Oszillatoren in Gegenwart von dem Treiben der globalen Kopplung effektiv bistabil werden, und sich so in zwei Gruppen organisieren. Das mittlere Feld, welches durch diese Gruppen aufgebaut wird, ist quasiperiodisch wodurch der Chimera Zustand sich selbst stabilisiert. In einem anderen Beispiel zeigen wir, dass der Chimera Zustand auch durch einen frequenzabhängigen Phasenunterschied in der globalen Kopplung erreicht werden kann.

Zur genaueren Untersuchung der Mechanismen, die zur effektiven Bistabilität führen, betrachten wir im zweiten Teil der Arbeit den Einfluss einer externen periodischen Kraft auf einzelne Oszillatoren mit zeitverzögerter Selbstkopplung. Wir führen die Stabilitätanalyse des synchronen Zustands durch, und stellen die Arnoldzunge dar.

Im dritten Teil der Arbeit stellen wir die Ergebnisse einer Synchronisationsanalyse vor, welche in Kooperation mit Wissenschaftlern der Psychologischen Fakultät der Universität Potsdam durchgeführt wurde. In dem Projekt wurde die Auswirkung des Herzrhythmus auf die menschliche Zeitwahrnehmung erforscht. Unsere Aufgabe war es, die experimentellen Daten statistisch zu analysieren. Im Experiment sollten Probanden ein gegebenes Zeitintervall reproduzieren während gleichzeitig ihr Herzschlag aufgezeichnet wurde. Durch eine Phasenanalyse haben wir den Zusammenhang zwischen dem Herzschlag und der Start- bzw. Stoppzeit der zu reproduzierenden Zeitintervalle untersucht. Es stellt sich heraus, dass Herzschläge bei Zeitintervallen über einige Sekunden als Taktgeber dienen können.

Contents

1. Introduction

Synchronization is a fundamental phenomenon [22, 55, 71]. Examples of it can be found in various natural systems of different size and level. Synchronization was first observed and described by Ch. Huygens in seventies century as he discovered that two mechanical clocks oscillate in opposite directions. Nowadays this phenomenon is well known and has found an application in synchronizing the clocks and frequency adjusting of electrical systems, as well as in bridge construction [44, 70]. Synchronization appears in mechanical systems, like musical instruments, in lasers, and in Josephson junctions [4, 20]. An interesting demonstration of synchronization effect is observed in periodic chemical reactions, e.g. in the Belousov-Zhabotinsky reaction [32]. In biological systems the synchronization emerges not only in the level of cells, e.g. in the circadian rhythm [47], but also among a large population, as the synchrony firing of fireflies. Moreover, the synchronous behaviour was found in cardiorespiratory coordination [63, 11], and in neuroscience. The model of phase oscillators and their synchronization are considered as one of the main models of interacting neurons [25, 12].

Synchronization phenomenon is essential for normal functioning of a live system. For example, in coordinated motion of body parts or in production of a macroscopic rhythm by synchronous firing of many cells, which governs respiration, heart contraction, and other rhythmic oscillations. Sometimes, synchronization leads to a pathology, e.g. in the case of the Parkinson's disease, when locking of many neurons results in tremor activity.

In this work we consider complex regimes of synchronization. We make theoretical modeling, numerical simulations, and use synchronization method to analyse experimental data.

Since Y. Kuramoto [33, 34] developed the phase approximation method as a general description for weakly coupled oscillators, a lot of works were dedicated to study dynamics of globally coupled oscillators. However, recently a lot of attention was attracted to the field of complex regimes between synchrony and asynchrony [76, 46, 61]. One of them is the regime of coexistence of coherence and incoherence in system of coupled oscillators [5, 35], which was called later as "chimera state" [2, 52, 66, 9, 36, 41, 83, 37, 85, 53] and was demonstrated in an experiment [51]. Some recent works [17, 64, 65] imply that chimera state is also possible in identical globally coupled oscillators. In the first part of this work, we investigate an example of this state, which we called chimera-like state, and answer the question, under which conditions this state emerges in identical globally coupled oscillators systems. We explain appearance and stability of chimera-

like state in our model. Also, we present another examples, where the chimera state appears due to frequency dependence of the phase shift.

In the second part of this work we inquire into the question, what is the role of the bistability of the oscillator with intrinsic delayed feedback in inducing chimera-like state. Therefore, we model influence of an external periodic force to the oscillator and analyse synchronization in the case of mono- and bistable state.

The property of phase oscillators to be synchronized even by a weak interaction make the synchronization analysis a useful method to reveal an influence of one oscillating system to another. This was used in the third part of this dissertation, where we present the results of the work, which was done in collaboration with our colleagues from the Psychology Department of the University of Potsdam. The aim of this research was to revel influence of body signals, like one's heartbeat on perception of time. We made statistical analysis of the experimental data and measured possible phase locking between cardiac cycle and time interval reproduction responses.

We continue the introduction with description of main synchronization concepts that are necessary to consider the problems discussed in other chapters. Let's start with the phase concept. Consider $N \geq 2$ dimensional dissipative autonomous system of ODE

$$\frac{d\mathbf{x}}{dt} = f(\mathbf{x}), \ \mathbf{x} = (x_1, x_2, \ldots, x_N), \tag{1.1}$$

with stable periodic solution with period T: $\mathbf{x}_0(t) = \mathbf{x}_0(t + T_0)$, Since the system is dissipative, the solution will be a limit cycle. By the index 0 we denote the solution along the limit cycle. We can introduce a coordinate along the limit cycle, that changes to 2π after each rotation, as a *phase* variable ϕ. This variable will obey the following equation

$$\frac{d\phi}{dt} = \omega_0, \tag{1.2}$$

where $\omega_0 = 2\pi/T_0$ will be referred as the *natural frequency* of the oscillator. In the presence of a small perturbation the system in Eq. 1.1 is described by

$$\frac{d\mathbf{x}}{dt} = f(\mathbf{x}) + \varepsilon \mathbf{p}(\mathbf{x}, t), \tag{1.3}$$

where the external force $\varepsilon \mathbf{p}(\mathbf{x}, t) = \varepsilon \mathbf{p}(\mathbf{x}, t+T)$ is periodic with the period T, in general different from T_0. If we introduce the phase in the vicinity of the limit cycle, then since the phase is a smooth function of the coordinate, one can write the equation of phase dynamics as [34, 55]:

$$\frac{d\phi}{dt} = \omega_0 + \varepsilon Q(\phi, t), \tag{1.4}$$

where

$$Q(\phi, t) = \sum_k \frac{\partial \phi(\mathbf{x_0}(\phi))}{\partial x_k} p_k(\mathbf{x_0}(\phi), t), \tag{1.5}$$

is a 2π-periodic function of the phase ϕ and a T-periodic function of t. Thus, one can represent Eq. 1.5 in the form of Fourier series. Then by averaging and leaving only resonance terms

$$k\omega_0 + l\omega \approx 0, \tag{1.6}$$

where k and l are integer numbers and $\omega = 2\pi/T$ is the frequency of the external force, one obtain an averaged equation for phase dynamics

$$\frac{d\phi}{dt} = \omega_0 + \varepsilon q(\phi - \omega t), \tag{1.7}$$

where q is a 2π periodic function of it arguments. In the simplest case the function q is represented by sin function.

By introducing a new variable ψ which is the difference between the phase of the oscillator and the external force $\psi = \phi - \omega t$, and substituting in Eq. 1.7 we have

$$\frac{d\psi}{dt} = -\nu + \varepsilon q(\psi), \tag{1.8}$$

where ν is the frequency detuning $\nu = \omega - \omega_0$ [55]. It is clear, that for some values of parameters ν and ε Eq. 1.8 will have a fixed solution, and the phase of the oscillator will rotate with the frequency of the external force, i.e. will be synchronized. It happens when $\varepsilon \min\{q\} < \nu < \varepsilon \max\{q\}$. The domain of parameters, where synchronization appears, called *synchronization region* and the typical form of it is called *Arnold tongue*.

If we have a system of two interacting oscillators, by providing the same procedure we obtain an equation for phase difference, similar to Eq. 1.8

$$\frac{d\psi_{mn}}{dt} = -\nu_{mn} + \varepsilon q(\psi_{mn}), \tag{1.9}$$

where $\psi_{mn} = m\phi_1 - n\phi_2$ the phase difference between two oscillators, and $\nu = m\omega_1 - n\omega_2$ frequency mismatch in $m : n$ resonance case.

In application of the synchronization analysis, to introduce the quantitative measurement of synchronization, one reproduce the phases of two different oscillations in the system, then by using the phase difference as a relative phase calculate the synchronization index [49]

$$\gamma_{mn}^2 = \langle \cos(\psi_{mn}) \rangle^2 + \langle \sin(\psi_{mn}) \rangle^2. \tag{1.10}$$

In the absence of synchronization between this two elements of the system the synchronization index γ will be 0. In contrast, the value of γ will tend to 1, if there are an interaction. For noisy systems it will never reach 1, and remain in some intermediate value.

Let's consider the simplest case for Eq. 1.9, i.e. $1 : 1$ resonance and $q(\psi) = \sin(\psi)$, then we obtain Adler's equation

$$\frac{d\psi}{dt} = -\nu + \varepsilon \sin(\psi). \tag{1.11}$$

Depending on the sign of ε we have two cases. First, if $\varepsilon > 0$, then the fixed value of the phase lies in $-\pi/2 < \psi < \pi/2$, and $\psi = 0$ for zero detuning $\nu = 0$. In this case the coupling between oscillators are called *attractive*. In contrary, if $\varepsilon < 0$, then fixed value lies in $\pi/2 < \psi < 3\pi/2$, and for similar oscillators ($\nu = 0$) the phase difference equals to π, i.e. in anti-phase to each other. In this case the coupling is called *repulsive*.

Another important model used in synchronization analysis is the model of Kuramoto [34], the simple model of N mutually coupled oscillators with different natural frequencies ω_k. The equation of dynamics is governed by

$$\frac{d\phi_k}{dt} = \omega_k + \frac{\varepsilon}{N} \sum_{j=1}^{N} \sin(\phi_j - \phi_k). \qquad (1.12)$$

One can introduce the complex mean field

$$Ke^{i\Theta} = \frac{1}{N} \sum_{j=1}^{N} e^{i\phi_k}, \qquad (1.13)$$

and rewrite Eq. 1.12 in the following form

$$\frac{d\phi_k}{dt} = \omega_k + \varepsilon K \sin(\Theta - \phi_k). \qquad (1.14)$$

The main feature of this model is that for some arbitrary frequency distribution $g(\omega)$ there will be a non-zero mean field with the central frequency $\bar{\omega}$ and an amplitude $K \neq 0$. All oscillators with the frequencies $|\omega - \bar{\omega}| \leq \varepsilon K$ will be entrained by the mean filed and synchronized. Whereas, other oscillators with frequencies $|\omega - \bar{\omega}| > \varepsilon K$ will have asynchronous solutions. Starting from some critical value of the coupling strength $\varepsilon = \varepsilon_{cr}$ the transition, similar to the second-order phase transition, happens and the amplitude of the mean field grows with the square root low: $K \sim (\varepsilon - \varepsilon_{cr})^{1/2}$.

2. Chimeralike state in globally coupled oscillators

In spite of over forty years of research pioneered by A. Winfree [79, 80] and Y. Kuramoto [33, 34], the dynamics of globally coupled oscillator populations remains a challenging issue, with applications ranging from laser and Josephson junction arrays to problems of bridge engineering and modeling of brain waves [4, 20, 44, 70, 25, 12]. In addition to the well-studied self-synchronization transition, of particular recent interest are complex states between synchrony and asynchrony [76, 46, 61]. However, a lot of attention have attracted regimes of the coexistence of coherence and incoherence in oscillators lattices [5, 35]. These states, also known as "chimeras", have been addressed in numerous theoretical studies [2, 52, 66, 9, 36, 41, 83, 37, 85, 53] and demonstrated in an experiment [51]. Furthermore, it has been shown that already two interacting populations of globally coupled identical oscillators can for some initial conditions exhibit symmetry breaking of synchrony, so that one population synchronizes whereas the other remains asynchronous [1, 54]; existence of such chimeras has been also confirmed experimentally [74, 40].

A natural question is under which conditions can such a symmetry-breaking into synchronous and asynchronous groups be observed in a completely homogeneous globally coupled population of identical oscillators.

In our work [84] we have demonstrated that chimera-like states appear for a minimal generalization of the popular Kuramoto-Sakaguchi phase model to the case of globally coupled identical phase oscillators with internal delayed feedback, and discussed the underlying mechanism of dynamically sustained bistability. In this chapter, for the most part, we consider the results obtained in [84]. We start with the brief introduction to the global coupling and the chimera state. Then we introduce our model, which demonstrate the state, reminiscent to classical chimera, and called chimeralike state. More detailed description of this state is presented in the section of numerical simulation results. Further, we give theoretical description to the chimeralike state, it's stability and qualitatively explanation, formulated as a dynamical sustained bistability. Finally, we give two other examples, where the chimeralike state can be observed.

2.1. Synchronization in ensemble of coupled oscillators

Even two oscillating objects which has a weak interaction can be synchronized. The natural expectation is the ensemble of oscillators and oscillatory media to be synchronized. Several examples can be found in the nature, like the synchronization of fireflies and the synchronous applauding of a large audience. They are the examples of the global, all-to-all, coupling in the ensemble of self-sustained oscillators.

Globally coupled self-sustained oscillators can be quite generally treated in the phase approximation [34]. In the simplest case of identical sine-coupled units such an ensemble of N units is described by the Kuramoto-Sakaguchi model [62]:

$$\dot{\varphi}_k = \omega + \frac{\varepsilon}{N} \sum_{j=1}^{N} \sin(\varphi_j - \varphi_k + \beta) = \omega + \varepsilon \mathrm{Im}(e^{i\beta} Z e^{-i\varphi_k}) , \qquad (2.1)$$

where φ are the oscillators' phases, $\varepsilon > 0$ is the coupling strength, β is the phase shift in the coupling, and

$$Z = Re^{i\Theta} = N^{-1} \sum_{k=1}^{N} e^{i\varphi_k} \qquad (2.2)$$

is the complex Kuramoto order parameter (complex mean field). The system is known to tend to the fully synchronous state $\varphi_1 = \varphi_2 = \ldots = \varphi_N$, if the coupling is attractive, i.e. $|\beta| < \pi/2$, and to remain asynchronous otherwise. Notice, that this model, in contrast to the Kuramoto model presented by Eq. 1.12, has identical oscillators with the same natural frequencies.

However, the global coupling is not the only one type of coupling. It can be nearest neighbours coupling in the chain, in two dimensional lattice or non-local coupling, where the interaction is defined as an integral over the neighbours and with the kernel, that decay with the distance. In the last type of coupling revealed complex spaciotemporal state, later called "chimera", which is the subject of the next section.

2.2. Chimera state

An interesting spaciotemporal state was first reported in the work [35], where oscillators on the ring were coupled by means of finite-range nonlocal coupling demonstrated the coexistence of coherence and incoherence states. The system splitted into two domains with different dynamics. The first domain consists of mutually synchronized oscillators, whereas the second domain was completely desynchronized. Later in the work [2], the name "chimera" was given to this new synchronization phenomenon. According to the ancient Greek mythology, the chimera was a monster with parts of the body from different animals, like the body of a goat, the head of a lion and serpent's tail.
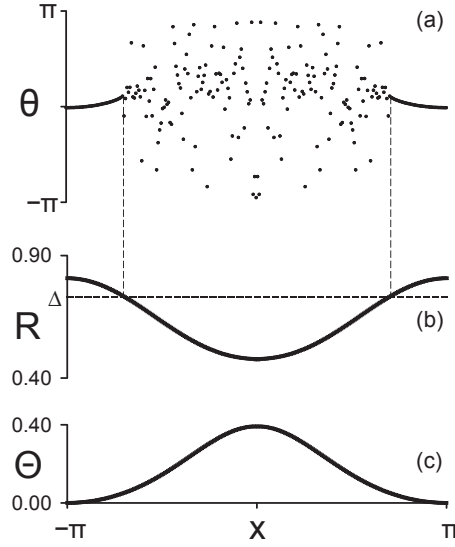
Figure 2.1.: Chimera state from [2]. (a) Phase pattern. (b) Local order parameter $R(x)$ defined by 2.4. (c) Local average phase $\Theta(x)$. Δ denotes frequency mismatch: $\Delta = |\omega - \Omega|$. Coherent solutions appear for the oscillators with coordinates x, where $R(x) \geq \Delta$. Drifting solutions take place where $R(x) < \Delta$.

The model considered in the works [35, 2] was the system of nonlocally coupled complex Ginsburg-Landau equations, which was reduced to a phase equation of the following form

$$\frac{\partial}{\partial t}\varphi(x,t) = \omega - \int G(x-x')\sin\left(\varphi(x,t) - \varphi(x',t) + \alpha\right)dx', \tag{2.3}$$

where $G(x-x')$ is the coupling function. By moving to rotating coordinates $\theta = \varphi - \Omega t$ and introducing the order parameter that depends on space and time

$$R(x,t)e^{i\Theta(x,t)} = \int G(x-x')e^{i\theta(x',t)}dx', \tag{2.4}$$

Eq. 2.3 is reduced to a forced one-oscillator equation

$$\frac{\partial}{\partial t}\theta(x,t) = \omega - \Omega - R\sin\left(\theta - \Theta + \alpha\right).$$

In Fig. 2.1 taken from [2] the chimera state and profiles of $R(x)$ and $\Theta(x)$ is shown. For the oscillators with coordinates x, where $|R(x)/(\omega-\Omega)| \geq 1$, the constant synchronized solution appears, while for other oscillators, where $|R(x)/(\omega - \Omega)| < 1$, the drifting solution takes place. In that way, the symmetry-breaking appears and the system of homogeneous oscillators splits into two groups with different dynamics.

2.3. The model

The main questions, addressed in this chapter are: (1) can chimera state be observed in the ensemble of globally coupled identical oscillators, and (2) what are the mechanism

behind the symmetry breaking if this state is possible.

In case of global coupling all oscillators are subject to the same force. Therefore, if the units are identical, one may expect that they should evolve similarly. This expectation is rather natural and is indeed true for simple systems like the standard Kuramoto model, as well as for many other examples from the literature. However, in a system of globally coupled identical chaotic maps, K. Kaneko observed one large synchronized cluster and a cloud of scattered units (see Fig 2b in [31]) – a state reminiscent of a chimera. For periodic units, namely for nonisochronous Stuart-Landau oscillators, such a state has been reported by Daido and Nakanishi [17] and Schmidt *et al.* [64], who studied the cases of linear and nonlinear global coupling, respectively, see also [65]. These observations that identical nonlinear elements behave differently in spite of being driven by the same force, indicate presence of bi- or multistability.

We consider a setup similar to Kuramoto-Sacaguchi model Eq. 2.1 for oscillators with an internal delayed feedback loop. The latter is a natural ingredient, e.g, of lasers with external optical feedback [42] and of numerous biological systems where signal transmission in the feedback pathway may be rather slow [23, 72, 7]. It is known, that phase dynamics of an autonomous oscillator with a delayed feedback loop can be in the simplest case represented as $\dot{\varphi} = \omega + \alpha \sin(\varphi_\tau - \varphi)$, where $\varphi_\tau \equiv \varphi(t - \tau)$, τ is the delay, and α quantifies the feedback strength [50, 42, 24]. Depending on the values of the parameters ω, τ and α the oscillator has one, two or multiple stable solutions. More detailed discussion of this oscillator we present in the chapter 3.1 .

Assuming the global coupling to be of the Kuramoto-Sakaguchi type as above, we write our basic model as

$$\dot{\varphi}_k = \omega + \alpha \sin(\varphi_{\tau,k} - \varphi_k) + \varepsilon \mathrm{Im}(e^{i\beta} Z e^{-i\varphi_k}) \, . \tag{2.5}$$

Here again Z is the complex Kuramoto order parameter (Eq. 2.2). The system of N equations 2.5 is formally infinite dimensional, since every oscillator is described by a nonlinear delay differential equation.

2.4. Results of numerical simulation, chimeralike state

In this section we show the results of numerical simulations and demonstrate a chimera-like state in model (2.5) mostly for parameter set $\omega = 1$, $\alpha = 1/3$, $\beta = \pi/2 + 0.01$, $\tau = \pi - 0.02$, $\varepsilon = 0.05$, and $N = 100$. It is noteworthy, that for this set of parameters the individual oscillator without coupling is in monostable state (see Fig. 2.6). Depending on the initial conditions and the parameter β the system reveal different states: fully synchronized state; desynchronized state, when all oscillators are desynchronized; chimeralike state, with one large synchronized cluster and a cloud of desynchronized
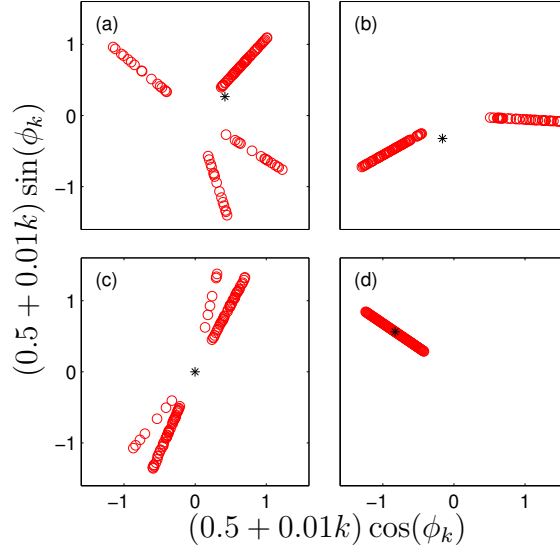
Figure 2.2.: Snapshot of phases for particular solutions of Eq. 2.5. The parameters of the system are: (a) $\beta = \pi/2 + 0.1$, $\varepsilon = 0.05$, $\tau = \pi - 0.02$; (b) $\beta = \pi/2 + 0.01$, $\varepsilon = 0.05$, $\tau = \pi - 0.1$; (c) $\beta = \pi/2 + 0.25$, $\varepsilon = 0.05$, $\tau = \pi - 0.01$; (d) $\beta = \pi/2 - 0.4$, $\varepsilon = 0.02$, $\tau = \pi - 0.1$. The oscillators are shifted by radial coordinate. The black star ($*$) depict the mean field.

oscillators; clustered state, when the system splits into several clusters (in every cluster oscillators are mutually synchronized) and a cloud of desynchronized oscillators.

Some particular states are shown in Fig. 2.2. In all four states the system has $n = 100$ oscillators. The initial conditions were defined with one mutually synchronized 40 element cluster and 60 desynchronized oscillators with different frequencies. In the panels (a) and (b) four and two clustered states are shown. In these examples all clusters have different number of elements. As a result, the mean field is always nonzero. This lead to irregular frequencies and quasiperiodic motion of the clusters. However, there is another state, that is shown in the panel (c). The system splits into symmetric sized clusters, as well as symmetric distribution of this clusters on the circle, thereby producing zero mean field and equal frequencies. For example, in the panel (c) two clusters have 7 elements and two other clusters have 43 elements, which rotate with the frequency 0.7987. Fully synchronized state is shown in the panel (d).

In Fig. 2.3 (a),(b) we show chimeralike state after transients in the dynamics are over; the snapshot and the time evolution of the phases clearly depict a synchronized cluster of 64 oscillators and a cloud of 36 asynchronous ones. Notice that throughout this example we number the oscillators in a way that units with indices $k = 1, \ldots, n$ are in the cluster, whereas units with $k = n + 1, \ldots, N$ belong to the cloud. The size of the cluster we denote as $q = n/N$. Temporal phase dynamics is further illustrated in Fig. 2.3 (c): for the elements in the cluster it is highly regular with a nearly constant instantaneous frequencies, while oscillators in the cloud are chaotic and their instantaneous frequencies strongly fluctuate. Moreover, individual frequencies in the cloud are only weakly correlated, so that the phase differences demonstrate many phase slips

9

and are unbounded. This irregularity is also reflected in the strong fluctuations of the cloud contribution to the mean field, to be compared with nearly constant contribution from the cluster (Fig. 2.3 (d)).
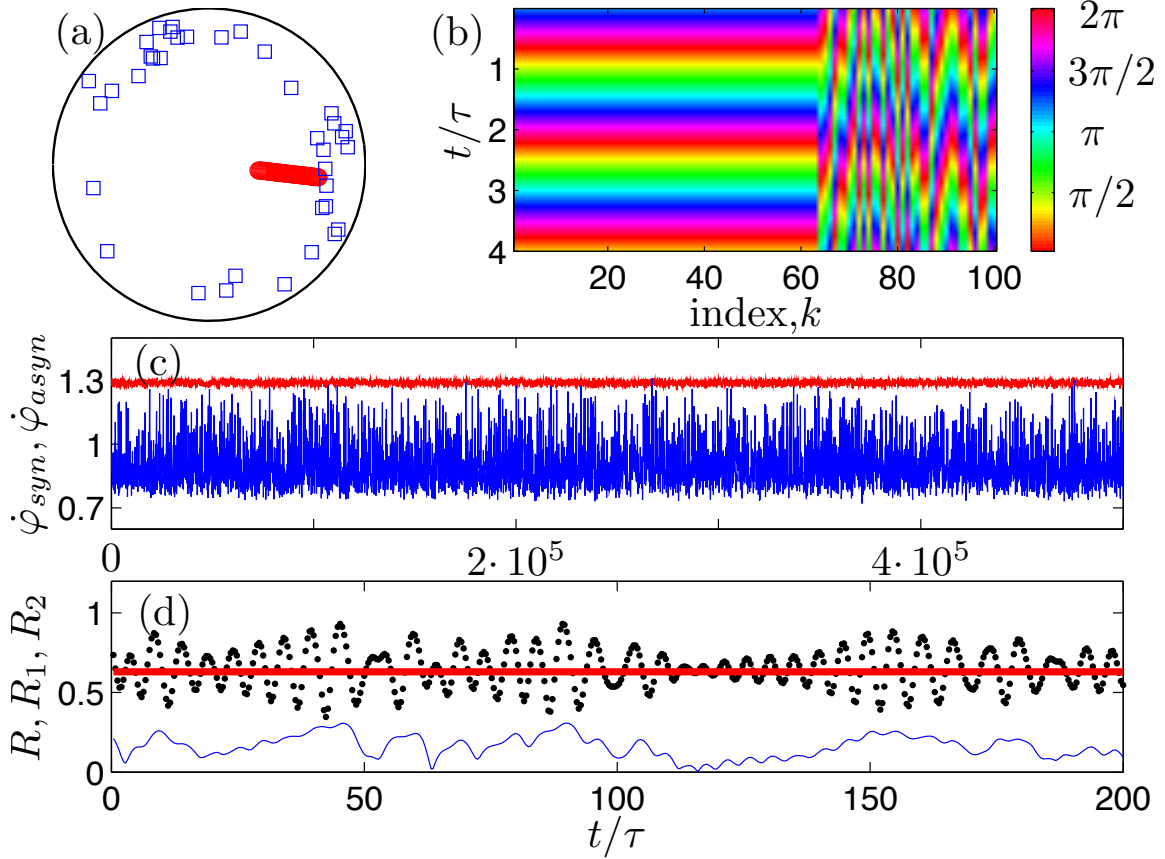

Figure 2.3.: Chimera state in model (2.5). The parameters of the system: $\omega = 1$, $\alpha = 1/3$, $\beta = \pi/2 + 0.01$, $\tau = \pi - 0.02$, $\varepsilon = 0.05$, and $N = 100$. (a) Snapshot of the phases reveals that 64 oscillators (red circles, numbered with $k = 1, \ldots, 64$) are in the cluster and 36 oscillators (blue squares) belong to the cloud. For visibility, the radial coordinate is increased proportionally to the oscillator index k. (b) Temporal evolution $\varphi_k(t)$, shown by color/grey coding. (c) Instantaneous frequencies of an oscillator from the cluster (upper red curve) and of an oscillator from the cloud (lower blue curve). The average values are $\langle \dot{\varphi}_{syn} \rangle_t = 1.2897$ (cluster) and $\langle \dot{\varphi}_{asyn} \rangle_t = 0.9033$ (cloud). (d) Amplitude of the mean field component contributed by the cluster, $R_1 = |\sum_{k=1}^{64} e^{\varphi_k}|/100$ (red bold line), and by the cloud, $R_2 = |\sum_{k=65}^{100} e^{\varphi_k}|/100$ (blue solid line). Black dotted line shows the amplitude R of the total mean field. From [84]

Formation of the chimera state is illustrated in Fig. 2.4 . Here in panel (a) we show the cluster growth for different initial conditions. For every run of this numerical experiment we changed the initial size of the cluster form $n = 30$ to $n = 60$ oscillators. All elements of the cluster had the same initial frequency and phase in the time range $[t_0, t_0 - \tau]$. The rest of the oscillators, i.e. the cloud elements, were places on the circle with random uniform distribution. The initial frequencies of the cloud elements were taken randomly between 0.7 and 1.2.

From the Fig. 2.4 we see that the cluster size saturates at a value between $n = 60$ and $n = 71$. Notice the logarithmic scale of the time axis: formation of the cluster with $q = n/N \approx 0.5$ is relatively fast, while its further growth is an extremely slow process. Below, in theoretical description (Chapter 2.5), we will show that the full synchrony state, i.e. the cluster with $q = 1$, cannot appear for choosen parameter set.

To show that formation of the chimera-like state is not a finite-size effect, in Fig. 2.4 (b) we illustrate formation of the chimera-like state for ensembles of different sizes, up to $N = 1000$. In all cases the final state has cluster of size $q \approx 0.6$. As shown below, for the stability of the chimera-like state it is important, that the fluctuation of the order parameter R_2 of the cloud does not vanish in the thermodynamic limit $N \to \infty$; Fig. 2.4 (c) demonstrates that the variance of R_2 practically does not depend on N up to values $N = 2000$. This fact indicates that the units of the cloud are not uncorrelated, but are organized in a collective chaotic mode. Finally, we emphasize that chimeras exist not only for parameters chosen above for an illustration, but in a finite parameter domain, shown in Fig. 2.5 together with domains of other types of dynamics.

2.5. Theoretical description

Next, we present theoretical arguments explaining existence of a chimera-like state in model (2.5). Let us consider first the fully synchronized, uniformly rotating one-cluster state $\varphi_1 = \ldots = \varphi_N = \Phi = \Omega t$, where frequency Ω is yet unknown. Substituting this expression into Eq. (2.5) we obtain

$$\Omega = \omega - \alpha \sin \Omega\tau + \varepsilon \sin \beta \ , \tag{2.6}$$

its solution $\Omega(\tau)$ is shown in Fig. 2.6, for cases $\varepsilon = 0$ (uncoupled oscillators) and $\varepsilon = 0.05$ (one-cluster state). We see that in both cases, the solution for the chosen delay τ is unique, i.e. there is no multistability. The fully synchronous cluster is, however, unstable. Indeed, consider a symmetric small perturbation to two arbitrary oscillators, $\varphi_{1,2} = \Phi \pm \delta$. Such a perturbation is transversal to the synchronization manifold and leaves the mean field unchanged; it obeys linearized equation

$$\dot{\delta} = \alpha \cos(\Omega\tau)(\delta_\tau - \delta) - \varepsilon\delta \cos \beta. \tag{2.7}$$

The detailed stability analysis of this linear delay differential equation we present in Appendix B, where we derive that the zero solution of Eq. B.1 (and correspondingly of Eq. 2.7) is unstable for $b = \varepsilon \cos \beta < 0$ (see Fig. 3.3). However, one can show that it is unstable with a simpler way: Most important is the eigenvalue which is close to zero; using its smallness we obtain in the first approximation $\lambda = -\varepsilon \cos \beta[1 + \tau\alpha \cos(\Omega\tau)]^{-1}$. Because for parameters used in Fig. 2.3 the quantity in brackets is positive, the fully synchronous state for $\varepsilon \cos \beta < 0$ is unstable. Physically, this means evaporation of the oscillators from the cluster. Numerical studies show that the fully asynchronous
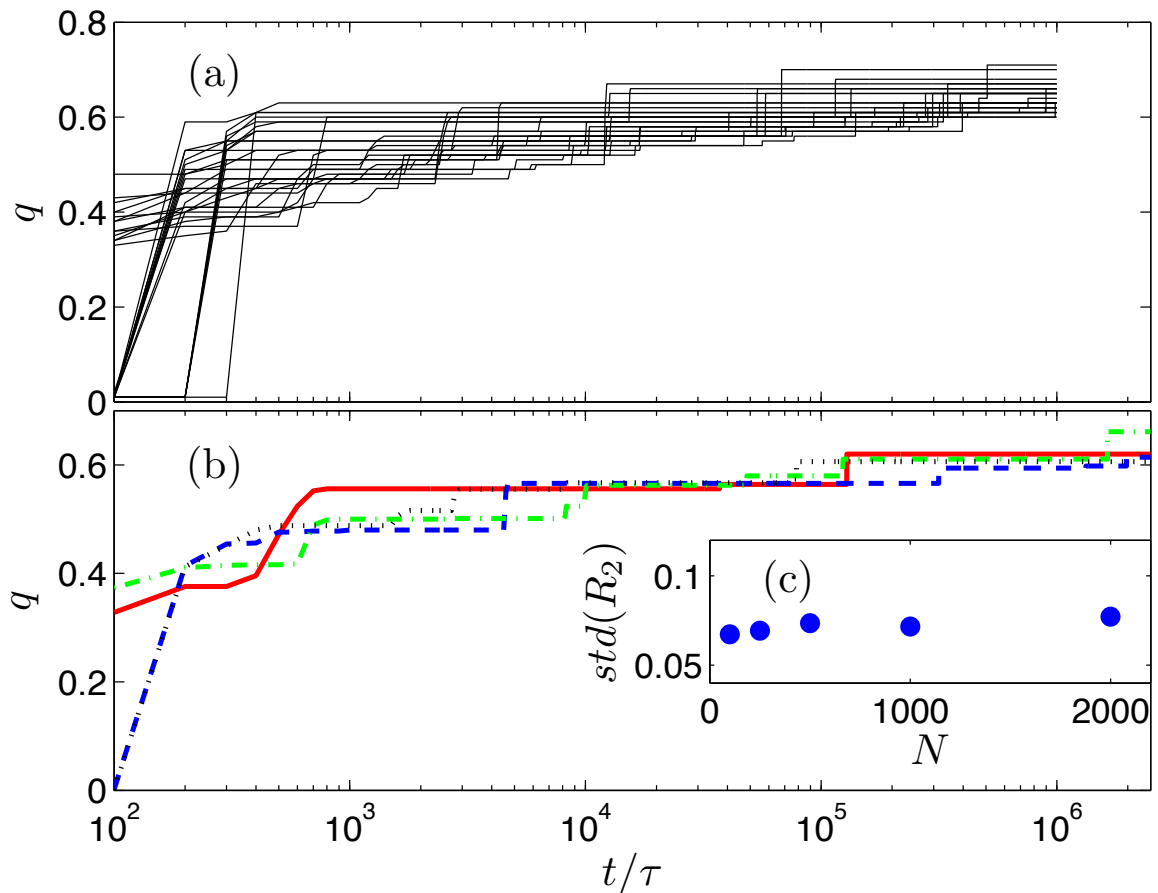
Figure 2.4.: Temporal evolution of the cluster and saturation of its size. (a) Growth of the relative cluster size $q = n/N$ for different initial conditions for $N = 100$ oscillators. (b) Saturation of q for different ensemble size: $N = 250$ (red solid), $N = 500$ (blue dashed), $N = 750$ (green dash-dotted), and $N = 1000$ (black dotted). (c) Standard deviation for the amplitude of the mean field component R_2 contributed by the cloud, for different ensemble size N.

state with uniform distribution of phases is unstable, too. Although we cannot exclude less trivial asynchronous states, i.e. with a non-uniform distribution of phases or with several clusters and zero mean field (see Fig. 2.2), we have not observed them for the chosen parameters.

A natural question is, why a partial cluster with $n < N$ elements (we denote its phase by Φ) is stable, while the full synchrony for $n = N$ is not. To analyze this, we again denote the perturbed phases of oscillators in the cluster as $\Phi \pm \delta$, and obtain after linearization (see detailed derivation in Appendix A):

$$
\begin{aligned}
\dot{\delta}(t) = & \ \alpha \cos(\Phi_\tau - \Phi)(\delta_\tau - \delta) - \\
& - \left[\frac{\varepsilon n}{N} \cos \beta + \frac{\varepsilon}{N} \sum_{j=n+1}^{N} \cos(\varphi_j - \Phi + \beta) \right] \delta.
\end{aligned}
\tag{2.8}
$$

Simultaneously we want to check, whether formation of another cluster via merging of oscillators from the cloud is possible. For this purpose we assume that two oscillators
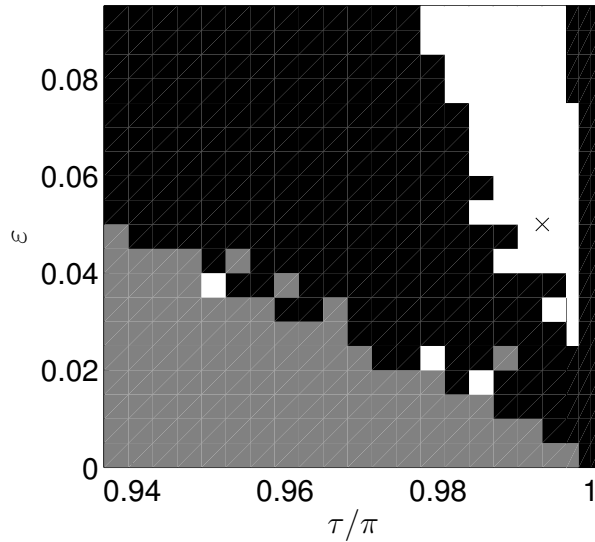
12

Figure 2.5.: Approximate domain of chimera states (white region); ω, α, and β are same as above, $N = 256$. Symbol $\times$ marks the parameters used in Figs. 2.3 , 2.4 . In the black domain we observed multi-cluster states, while the gray domain corresponds to the states with zero mean field and equal rotation frequencies for all units. The initial conditions were defined with the cluster of the size $q = 0.4$ and a cloud of desynchronized oscillators with different frequencies. From [84].
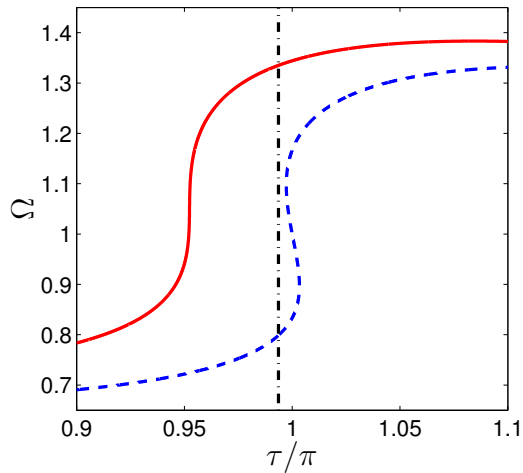
Figure 2.6.: Solution of Eq. (2.6): frequency of the one-cluster state Ω as function of τ, for uncoupled oscillators, $\varepsilon = 0$, (blue dashed line) and for $\varepsilon = 0.05$ (red bold line). Vertical black dash-dotted line marks $\tau = \pi - 0.02$. From [84] .

in the cloud come close to each other, so that $\Delta(t) = \varphi_k - \varphi_l$, $l, k > n$, is small, and we can linearize the corresponding equations to obtain for the difference (see detailed

derivation in Appendix A)

$$\dot{\Delta}(t) = \alpha \cos(\varphi_{l,\tau} - \varphi_l)(\Delta_\tau - \Delta) -$$
$$- \left[\frac{\varepsilon n}{N} \cos(\Phi - \varphi_l + \beta) - \frac{\varepsilon}{N} \sum_{j=n+1}^{N} \cos(\varphi_j - \varphi_l + \beta) \right] \Delta. \qquad (2.9)$$

We cannot solve Eqs. (2.8,2.9) analytically, as $\varphi_j(t)$ are unknown irregular functions of time. However, we solve this linear delay differential equations with varying coefficients numerically for large time interval T together with the full system (2.5) and compute the corresponding Lyapunov exponents

$$\lambda = \lim_{T \to \infty} \frac{\ln \delta(T)}{T} \approx -1.25 \cdot 10^{-2},$$

and

$$\Lambda = \lim_{T \to \infty} \frac{\ln \Delta(T)}{T} \approx 2.38 \cdot 10^{-2}.$$

Because the Lyapunov exponent λ describing transversal stability of the cluster is negative, and the exponent Λ describing transversal stability in the cloud is positive, the cluster is stable towards evaporation of the oscillators, while merging of cloud oscillators to another mini-cluster is forbidden.

Stabilization of the cluster can be qualitatively explained as follows. Contrary to the fully synchronized case, in presence of a cloud, oscillators in the cluster are subject to a force which has two components, as illustrated by Fig. 2.3 (d): a regular force from the cluster ($\epsilon q \sin(\beta) = $ const) and an irregular one from the cloud, which is proportional to $\epsilon(1 - q)$

$$\dot{\Phi} = \omega + \alpha \sin(\Phi_\tau - \Phi) + \epsilon q \sin(\beta) + \epsilon \frac{1}{N} \sum_{j \in cloud} \sin(\phi_j - \Phi + \beta). \qquad (2.10)$$

In the first approximation, the irregular component can be treated as a random force, and this effective noise is common for all elements of the cluster. It is known that common noise tends to synchronize oscillators [55, 10]. Here, for sufficiently strong noise, this tendency to synchrony overcomes the internal repulsion in the cluster and stabilizes it. However, the cluster cannot absorb all elements, because for $n = N$ the noisy component vanishes; hence, $n < N$.

Considering now the system from a different viewpoint, we discuss, why the periodic forcing from the cluster does not entrain the cloud oscillators and they eventually do not join the cluster. Indeed, at initial state of chimera formation more and more oscillators join the cluster (see Fig. 2.4) and the more oscillators merge into the cluster, the stronger is the forcing on the cloud oscillators. Hence, one may expect the increased tendency to synchrony. However, the size of the cluster always saturates between $q = 60$ and $q = 71$ (see Fig. 2.4).

In order to answer to this question in the chapter 3 we considered synchronization of an individual oscillator with delayed feedback loop by a periodic force, which corresponds to the cluster (Eq. 3.1). We show there that the synchronization appears in some area of the parameters space (see Fig. 3.5). If the frequency of the cluster is outside of this domain, the oscillator is not captured by the cluster and the cluster size stops growing.

Thus, with increase of n, the frequency of the cluster grows as described by $\Omega = \omega - \alpha \sin \Omega \tau + \varepsilon \frac{n}{N} \sin \beta$, where in the first approximation we neglect the random forcing from the cloud in Eq. 2.10 . For $n = 64$ the estimated frequency is $\Omega = 1.2901$, in a perfect agreement with the observed value 1.2897 (see Fig. 2.3 (c)). Hence, not only the amplitude $\varepsilon n/N$ of the forcing on non-synchronized units grows with n, but also the frequency mismatch. The growth of the cluster saturates when these values drift outside of the synchronization domain for the forced oscillators in the cloud. To confirm this, we have used the result of the chapter 3.2 and determined the synchronization domain for chosen parameters using a periodic forcing with parameters taken from the cluster dynamics. In Fig. 2.7 one can see that the forcing with the cluster frequency and the corresponding amplitude lies almost exactly at the border of the domain. Thus, the further entrainment of oscillators by the cluster is not possible.
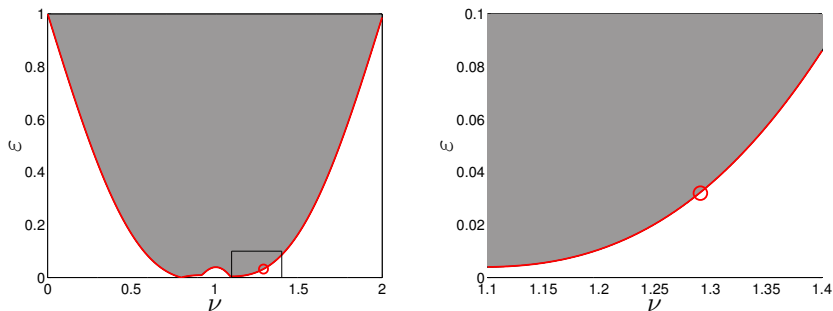

Figure 2.7.: The synchronization region for Eq. 3.2 (gray). The theoretically found border of synchronization region shown by red line. Red circle, which corresponds to the values of the cluster frequency and corresponding amplitude $(\omega_{cl}, \epsilon q)$ obtained by the numerical simulation, lies almost exactly at the border of the synchronization region. The right plot is the enlarged view of the left plot. From [84].

Presented discussion explains the mechanism of the *dynamically sustained bistability* that underlies the chimera-like state in our globally coupled system of identical units: the ensembles splits into two parts with completely different dynamics, and these parts together create a mean field that allows such a bistability. This mechanism is nontrivial, because, as illustrated in Fig. 2.6, for the chosen parameters the uncoupled systems are monostable. However, due to interaction, the oscillators become effectively bistable: being forced by the same field they exhibit two very different dynamical patterns. The oscillators in one group are regular and therefore easily synchronize with each other, while the others are highly irregular and remain in different asynchronous, although correlated, states. The global field that leads to the bistability is dynamically sustained in a self-consistent way.

2.6. Other examples of chimeralike state

Next we discuss less nontrivial, though more transparent, setups where already non-coupled oscillators are bistable. Here the coupling is organized in a way, that it acts repulsively on the oscillators in one state and attractively on those which are in the other state. For the first example we consider a model

$$\dot{\varphi}_k = \omega + \alpha \sin(\varphi_{\tau,k} - \varphi_k) + \varepsilon R \sin(\Theta_{\mathcal{T}} - \varphi_k + \beta) , \qquad (2.11)$$

where $Re^{i\Theta} = Z$ and $\Theta_{\mathcal{T}} = \Theta(t - \mathcal{T})$. In contradiction to our model (2.5), here not only individual oscillators possess a delayed feedback loop, but the global coupling is also delayed, with another delay time $\mathcal{T} \neq \tau$. Parameters of oscillators are taken as $\omega = \pi$, $\tau = 0.99$, and $\alpha = 1.2$, so that uncoupled units oscillate either with the frequency $\Omega_1 = 2.0845$ or $\Omega_2 = 4.0795$, i.e. are bistable. For coupling parameters $\varepsilon = 0.1$, $\beta = \pi/2$, and $\mathcal{T} = 0.2\tau$ we observe a chimera state (see Fig. 2.8), what can be explained as follows. Suppose there is a non-zero mean field with the frequency ν. In the first approximation, the delay in the coupling is equivalent to the phase shift $\nu\mathcal{T}$ which sums with the constant phase shift parameter β. The coupling is attractive if the total shift obeys $|\nu\mathcal{T} + \beta| < \pi/2$, and repulsive otherwise. Since the phase shift is frequency-dependent, the effective coupling through the same global mean field is attractive for individual oscillators having frequency $\nu = \Omega_1$ and repulsive for those with $\nu = \Omega_2$. As a result, the sub-population of oscillators which initially are in the state with Ω_1 synchronize, while the elements with Ω_2 remain asynchronous. Indeed, after the transient in the system is over the mean field produced by desynchronized oscillators is almost zero. Thus, the mean field will be defined only by the cluster elements. The cluster and the mean filed will be phase locked with phase difference $|(\Omega_1 - \omega)\mathcal{T} + \pi/2| = |(\Omega_1 - \omega)\tau \cdot 0.2 + \pi/2| = 1.3615 < \pi/2$. In contrary, the phase of the oscillator with frequency Ω_2 the phase shift will be $|(\Omega_2 - \omega)\tau \cdot 0.2 + \pi/2| = 1.7565 > \pi/2$.
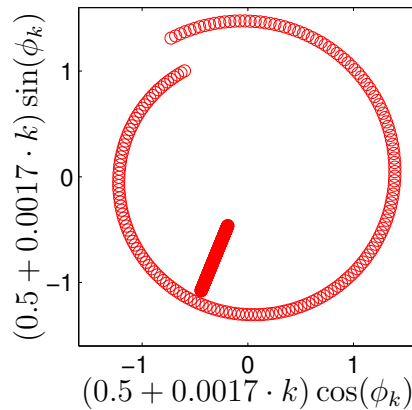

Figure 2.8.: Phase snapshot of the chimera state in the system Eq. 2.11. Clearly seen the synchronized cluster and desynchronized group of oscillators. To distinguish the oscillators the radial coordinates were shifted proportional to their index k.
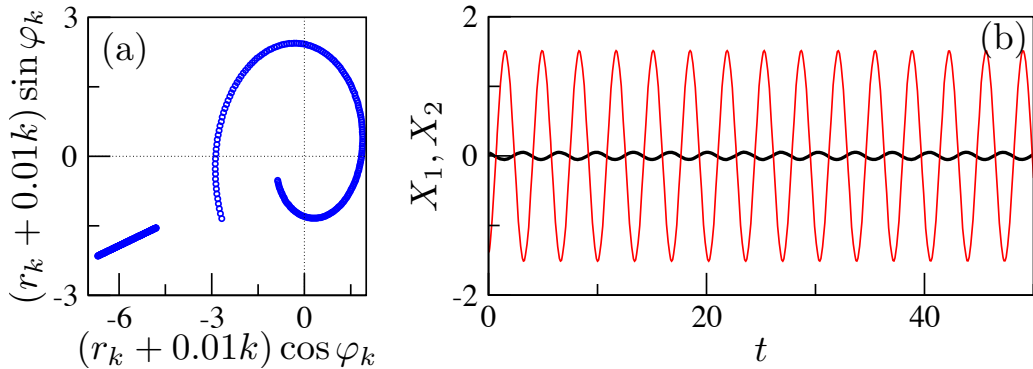
Figure 2.9.: Chimera state in the system of identical Stuart-Landau type oscillators Eq. (2.12). (a) Snapshot clearly demonstrates one cluster and a group of asynchronous units. Notice that for visibility, in the plot the amplitudes of all units are substituted as $r_k \to r_k + 0.01k$. (b) Mean fields of two subgroups, $X_1 = N^{-1} \sum_{j=1}^{N/2} r_k \cos \varphi_j$ (bold black line) and $X_2 = N^{-1} \sum_{j=N/2+1}^{N} r_k \cos \varphi_j$ (solid red line). From [84]

A similar scenario can be implemented with bistable identical oscillators without delays. Consider N Stuart-Landau type oscillators, (here written in polar coordinates r_k, φ_k) having two stable limit cycles and let these oscillators be globally coupled via an additional linear circuit, described by variable u:

$$
\begin{aligned}
\dot{r}_k &= 0.1 r_k (1 - r_k^2)(4 - r_k^2)(9 - r_k^2) + \varepsilon \dot{u} \cos \varphi_k , \\
\dot{\varphi}_k &= 1 + \alpha r_k^2 - \varepsilon \frac{\dot{u}}{r_k} \sin \varphi_k , \\
\ddot{u} + \gamma \dot{u} + \eta^2 u &= N^{-1} \sum_{j}^{N} r_j \cos \varphi_j .
\end{aligned}
\tag{2.12}
$$

Parameters are $\alpha = 0.1$, $\varepsilon = 0.1$, $\gamma = 0.01$, $\eta = 1.5$, $N = 400$. In the simulation, initially $N/2$ units were close to the limit cycle with the amplitude ≈ 1 whereas the others were close to the second limit cycle, with the amplitude ≈ 3. The observed chimera state is shown in Fig. 2.9 . Indeed, the frequencies of the limit cycle oscillations are $\Omega_1 = 1.1$ and $\Omega_2 = 1.9$. Since the resonant frequency of the circuit η lies between them, $\Omega_1 < \eta < \Omega_2$, the phase shift in the global coupling introduced by the harmonic circuit is attractive for the state with Ω_2 and repulsive for that with Ω_1.

2.7. Summary

In summary, we have demonstrated numerically and explained semi-quantitatively the emergence of chimera states in ensembles of identical globally coupled oscillators. We have outlined a mechanism of dynamically sustained bistability which results in symmetry-breaking of the initially homogeneous system. Here, a remarkable constructive role is played by collective chaos of non-synchronized units: the irregular forcing

from the cloud counteracts the instability of the fully synchronous state, thus stabilizing the cluster of synchronized $n < N$ elements. We have also demonstrated that chimera-like states are possible without this mechanism, if the individual units are naturally bistable, like in setups described by Eqs. (2.11 ,2.12). We stress that the chimera-like regimes here are conceptually much simpler than in the model (2.5): the asynchronous oscillators are not chaotic; moreover, here the partition into synchronous and asynchronous states is fully determined by initial conditions, while in Eq. (2.5) the partition appears self-consistently.

In this chapter we analyzed only ensembles of identical oscillators, as here the effect is mostly striking. However, we expect that the main features survive for small heterogeneity and/or noise; this issues remain a subject of a future study.

3. Phase synchronization of an oscillator with delayed feedback by external force

As it was shown in the previous chapter, globally coupled oscillators with internal delayed feedback can reveal non trivial states, like chimeralike and clustered states. Coexistence of a coherent and incoherent domains in chimeralike state was explained by dynamically sustained bistability. Initially small amount of mutually synchronized oscillators build a cluster. By absorbing other oscillators the cluster starts growing. However, when the cluster reaches the certain size it can not capture new elements, and the system does not reach the fully synchronized state. To understand the saturation of the cluster in the level of the individual oscillator we consider the synchronization of the oscillator with internal delayed feedback with the cluster. In the first approximation the cluster with constant mean frequency can be replaced by external periodic force.

We represent our model in the following form

$$\dot{\phi} = \omega + \alpha \sin(\phi_\tau - \phi) + \varepsilon \sin(\nu t - \phi). \tag{3.1}$$

Here ω is the natural frequency of the oscillator, τ and α are delay and strength of the internal feedback loop. Parameters of the external force are its strength ε and frequency ν, which is assumed to be close to ω. The interaction with the external force is taken as a sine of the phase difference.

One can rewrite this equation introducing the phase difference to that of the external force, i.e. $\psi = \phi - \nu t$:

$$\dot{\psi} = \dot{\phi} - \nu = 1 - \nu + \alpha \sin(\psi_\tau + \nu t - \nu \tau - \psi - \nu t) - \varepsilon \sin(\psi).$$

Finally we have

$$\dot{\psi} = 1 - \nu + \alpha \sin(\psi_\tau - \psi - \nu \tau) - \varepsilon \sin(\psi). \tag{3.2}$$

In this chapter we start with an individual oscillator and it's properties. Next, we find the synchronization region in general case. Finally, we consider two modes of the oscillator and discuss bistable and hysteretic features of their Arnold tongues.

3.1. An oscillator with intrinsic delayed feedback

An autonomous oscillator with delayed feedback loop can be reduced to a phase model. In the simplest case the delayed feedback loop is represented as a sine function, i.e. the first term of Fourier set [50, 42, 24]:

$$\dot{\varphi} = \omega + \alpha \sin(\varphi_\tau - \varphi), \tag{3.3}$$

where τ is the delay, $\varphi_\tau \equiv \varphi(t - \tau)$, and α quantifies the feedback strength. The intrinsic delayed feedback can appear in a natural manner in several biological systems [42, 72], in gene-oscillators [43, 69], in human physiological systems, namely control systems [6], in lasers with opto-electronic feedback [21], and in mechanical systems [19].

The monotone growing solution of Eq. 3.3 lead to the following relation

$$\Omega = \omega - \alpha \sin(\Omega \tau). \tag{3.4}$$

This equation for $|\alpha\tau| > 1$ has, depending on the value of τ, one, two or multiple stable solutions $\varphi_{1,2} = \Omega_{1,2} t$ (see Figs. 3.1, 3.2).

The turning point of the curve $\Omega(\tau)$ can be easily found. It appears when the derivative $d\Omega/d\tau = \infty$. Indeed, if we rewrite the Eq. 3.4 and define the curve $\Omega(\tau)$ as a parametric function

$$F(\Omega, \tau) = \Omega - 1 + \alpha \sin(\Omega \tau) = 0,$$

then the derivative will be

$$\frac{d\Omega}{d\tau} = -\frac{\frac{\partial F}{\partial \tau}}{\frac{\partial F}{\partial \Omega}} = -\frac{\alpha \cos(\Omega \tau)}{1 + \alpha \tau \cos(\Omega \tau)}.$$

If the feedback strength $\alpha = 1/\pi$ then $d\Omega/d\tau = \infty$ at $\tau = \pi$ (see Fig. 3.1).

To have a bistable mode in $\Omega(\tau)$ we take the value of the feedback strength as $\alpha = 1/3 > 1/\pi$. Further we will consider two modes of the oscillator Eq. 3.3: the first one is the symmetric case with $\tau = \pi$. In this mode there are two stable solutions with frequencies $\Omega_1 = 0.8333(3)$ and $\Omega_2 = 1.1666(6)$. The second case is called asymmetric, with $\tau = \pi - 0.02$, where only one stable solution with frequency $\Omega_* = 0.7987$ exists. They are shown in Fig. 3.2.

Notable, that in a real system the delay is not have to be so large like π. The combination of ω, α and τ defines whether the oscillator is in one-, bi- or in multi-stable mode. The choice of the parameters value were guided by convenience in theoretical calculations.
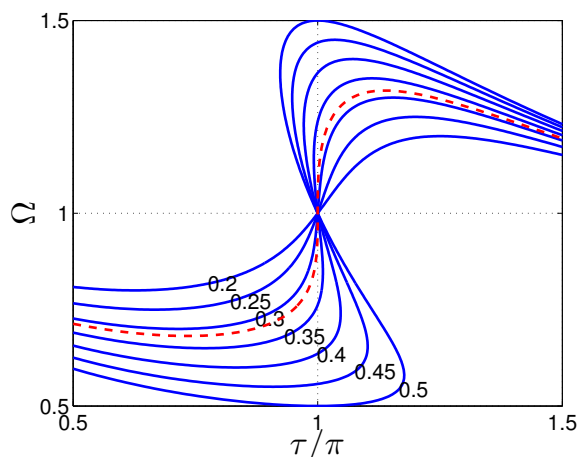
Figure 3.1.: Representation of the transition from mono to bistable mode of the oscillator Eq. **??**. The blue solid lines are the dependence of the frequency Ω on the delay τ in Eq. 3.4 for $\omega = 1$ and different values of α (shown as numbers). The red dashed line corresponds to the value of $\alpha = 1/\pi$, where bistability appears.

3.2. Synchronization by external periodic force

In this section we find the region of parameters where the oscillator is synchronized by the external force, i.e. we construct Arnold tongue. Therefore we consider the stability of the phase locked state of Eq. 3.2.

If the oscillator is synchronized with the external force and $\psi(t) = \psi_0 = \text{const}$ then form Eq. 3.2 we obtain

$$0 = 1 - \nu - \alpha \sin(\nu\tau) - \varepsilon \sin(\psi_0). \tag{3.5}$$

Linearization around the solution ψ_0 gives

$$\dot{\delta} = \alpha \cos(\nu\tau)(\delta_\tau - \delta) - \varepsilon \cos(\psi_0)\delta. \tag{3.6}$$

if we denote

$$a = \alpha \cos(\nu\tau) \ \text{ and } \ b = \varepsilon \cos(\psi_0) = \sqrt{\varepsilon^2 - (\nu + \alpha \sin(\nu\tau) - 1)^2}, \tag{3.7}$$

we obtain a linear delay differential equation

$$\dot{\delta} = a\delta_\tau - (a + b)\delta.$$

The stability of this equation is discussed in Appendix B. The stability chart is shown in Fig. 3.3.

Using this results and Eq. 3.5 we find stability of the phase locked solution for Eqs. 3.2:

1. First condition comes from the fact that the phase ψ_0 is a real number:

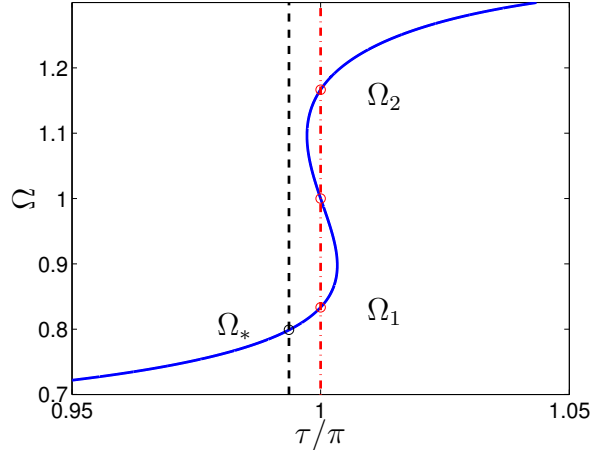$$\varepsilon \geq |(\nu + \alpha \sin(\nu\tau) - 1)|. \tag{3.8}$$

Figure 3.2.: An example of bistable solution of Eq. 3.4: The frequency of an oscillator Ω (Eq. 3.3) is presented as a function of τ for $\omega = 1$, $\alpha = 1/3$. The vertical black dashed line is $\tau = \pi - 0.02$, and vertical red dash-dotted line is $\tau = \pi$. In the first case there is only one stable solution (the black circle) with the frequency $\Omega_* = 0.7987$, whereas in the second case there are two stable solutions: lower $\Omega_1 = 0.8333$ and upper $\Omega_2 = 1.16666$ (red circles); and one unstable solution with $\Omega = 1$ (middle red circle).
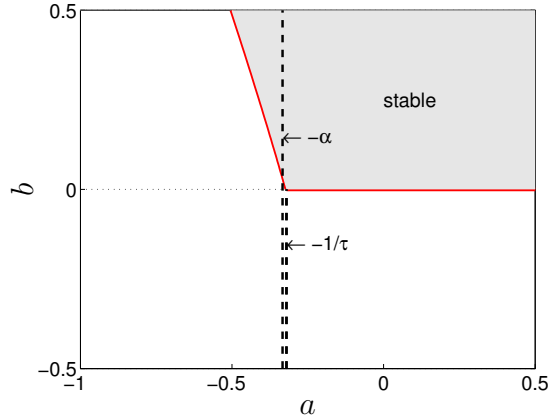
Figure 3.3.: Stability chart for zero solution of the linear delay differential equation (Eq. B.1, see Appendix B) enlarged around origin. The border of the stability region (gray colored) is given by two red curves: the horizontal line ($b = 0$) and the left curve starting from $(a, b) = (-1/\tau, 0)$, which is given as a parametric function of ω: $a(\omega) = -\frac{\omega}{\sin(\omega\tau)}$, $b(\omega) = \omega \tan(\omega\tau/2)$, $\omega \in [0, 1]$.

2. From the stability conditions of Eq. B.1, we have:

   - if $\varepsilon \cos(\psi_0) < 0$ the solution is unstable.

   - if $\varepsilon \cos(\psi_0) \geq 0$ and $\alpha < 1/\tau$, then system is stable. (See Fig. 3.3)

   - if $\alpha > 1/\tau$ and $\varepsilon \cos(\psi_0) \geq \omega_1 \tan(\omega_1\tau/2)$, where ω_1 is the solution for $\omega_1 - \alpha \sin(\omega_1\tau) = 0$, then the solution is stable

   - if $\alpha > 1/\tau$ and $\varepsilon \cos(\psi_0) < \omega_1 \tan(\omega_1\tau/2)$, where ω_1 is the solution for $\omega_1 - \alpha \sin(\omega_1\tau) = 0$, then if $\alpha \cos(\nu\tau) > -\omega_2/\sin(\omega_2\tau)$, where ω_2 is the solution

for $\varepsilon \cos(\psi_0) = \omega_2 \tan(\omega_2 \tau/2)$, the constant solution is stable. Otherwise unstable.

In other words, the main stability condition is Eq. 3.8. Due to the fact that in our case $b = \varepsilon \cos(\psi_0) \geq 0$, and $\alpha > 1/\tau$, we have extra conditions (See Fig. 3.3): Two vertical dashed lines in Fig. 3.3 show the minimal value of $a = -\alpha$ and the value of $-1/\tau$. To the left of $-1/\tau$ the Hopf bifurcation curve starts. If we change the parameter ε and ν according to Eq. 3.8 we will have corresponding nontrivial curve in the parameters plane (a, b). When $\alpha < 1/\tau$, then the curve never crosses the bifurcation curve. And if $\alpha > 1/\tau$, which is in our case, the Hopf bifurcation can appear. We can find the points where the curve Eq. 3.8 crosses the bifurcation curve and correct the value of ε for that region (See Appendix C for details). Thus, for

$$\nu \in \left[\frac{\arccos(-1/(\alpha\tau))}{\tau}, \frac{2\pi - \arccos(-1/(\alpha\tau))}{\tau} \right],$$

the value of ε should be corrected and obey

$$\varepsilon > \sqrt{\left(\omega(\nu) \tan\left(\frac{\omega(\nu)\tau}{2}\right)\right)^2 + (\nu + \alpha \sin(\nu\tau) - 1)^2}, \qquad (3.9)$$

where $\omega(\nu)$ can be found from

$$\omega(\nu) + \alpha \cos(\nu\tau) \sin(\omega(\nu)\tau) = 0,$$

and $\omega(\nu) \in [0, \omega_{max}]$, where ω_{max} is the solution of the equation

$$\omega_{max} - \alpha \sin(\omega_{max}\tau) = 0.$$

The stability regions for $\tau = \pi$ and $\tau = \pi - 0.02$ is shown in Fig. 3.4 (b) and Fig. 3.5 (b) for the symmetric ($\tau = \pi$) and asymmetric ($\tau = \pi - 0.02$) cases correspondingly. More discussion of this cases will be in the next section.

3.3. Arnold tongues

We carried out numerical simulations by solving the Eq. 3.2 for different initial conditions and different values of ν and ε. The predictor-corrector integration method for delay differential equations was used to find the solution of Eq. 3.2.

By calculating the mean value of the frequency $\dot{\psi}$ and it's root mean square one can find the regions of the phase locked synchronization and frequency locked synchronization. In the first case both values are zero. These points are shown as gray points in Fig. 3.4 (b), and Fig. 3.5 (b). The second case appears, when the phase is periodically oscillating around some constant value, so that the mean of the frequency is the same as the

frequency of the external periodic force. Thus in the coordinates of the periodic force the mean frequency is zero. Whereas, the root mean square is not equal to zero. These points are shown with red points in Figs. 3.4 (b), 3.5 (b). They correspond to the solutions that appear after Hopf bifurcation. The frequency $\dot{\psi}$ of typical solutions are shown in Fig. 3.6. In Figs. 3.4 (a), 3.5 (a), and Fig. 3.6 (d) the color plots were obtained by smoothing procedure of the `MatLab` function `surface()` applied to the numerical results. The original grid steps were 0.005 in both axes ν and ε. The typical realizations of $\dot{\psi}$ of the solutions of Eq. 3.2 for asymmetric case is shown in the Fig. 3.6.

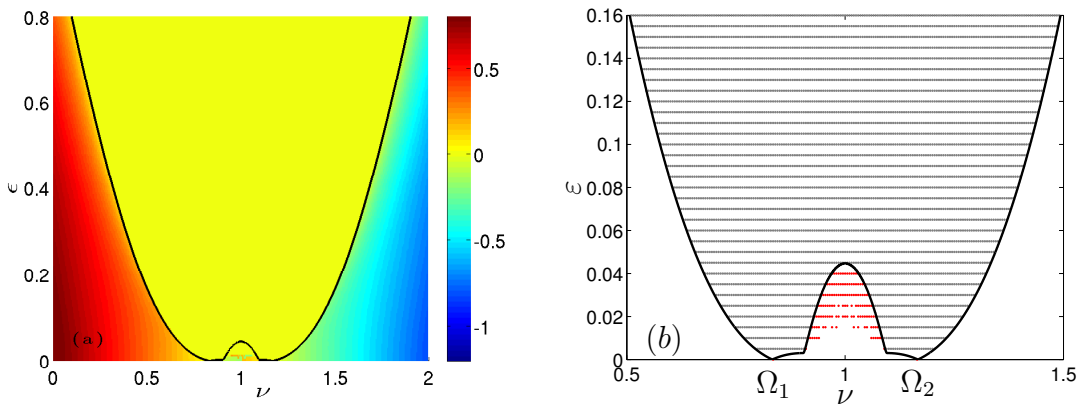## 3.3.1. Symmetric case $\tau = \pi$

Figure 3.4.: Arnold tongue for symmetric case ($\tau = \pi$). The black lines show theoretically found border of the synchronized state. (a) Mean value of $\dot{\psi}$ on the (ν, ϵ) plane coded by color. (b) The fully synchronized states obtained by numerical simulation are marked with the gray points, the synchronized states with varying phase difference (after Hopf bifurcation) are marked with the red points. The white region is desynchronized states (periodic solutions).

In the symmetric case the oscillator (Eq. 3.3) without external force is bistable and has two stable solutions with frequencies: $\Omega_1 = 0.8333$ and $\Omega_2 = 1.1666$ (See Fig. 3.2).

The result of numerical simulations shown in Fig. 3.4 agree with the theoretical calculations. In the Arnold tongue for this case (Fig. 3.4 (b)) has two edges "touching" the ν axes exactly on the values of the stable frequencies Ω_1 and Ω_2. In the middle, the Hopf bifurcation curve defined by Eq. 3.9 divide the synchronized solution from periodic solution with zero mean (see Fig. 3.5 (g)). This solution loose the stability as ε tends to zero. Outside of the tongue the Eq. 3.2 has periodic solution, similar to those shown in Figs. 3.6 (a), (c), (e). When the parameters come close to the border of the Arnold tongue the period of the oscillators frequency increases (Fig. 3.6 (c)), and synchronization emerges by extending of the period to infinity. The transition of the periodic solutions remains continues, during the change of the value of ε from small to high and backward.

3.3.2. Asymmetric case, $\tau = \pi - 0.02$

The results of the numerical simulations and theoretical calculations for this case shown in Fig. 3.5. Similar to the previous case, the black line denotes the theoretically found border of the synchronized solution, which are shown with the gray points. The red points indicate the frequency locked solutions. It is need to be mentioned, that this numerical results was obtained with initial conditions corresponding to synchronized state with small perturbation.
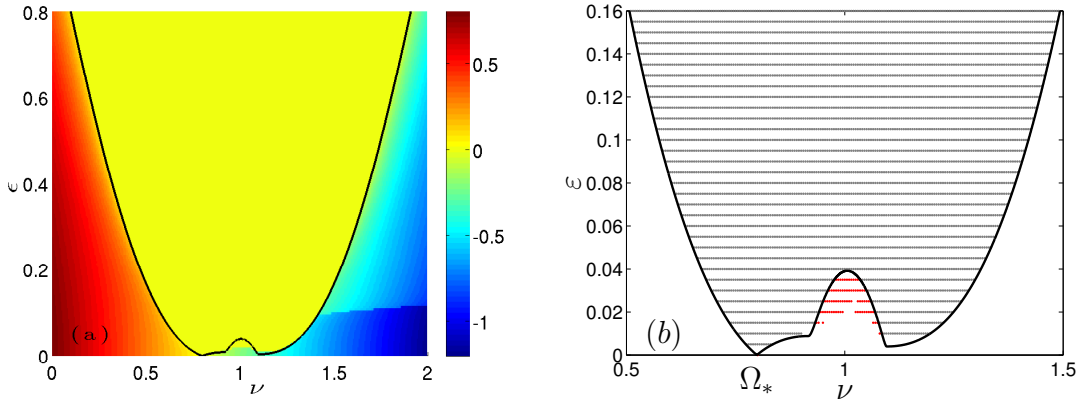

Figure 3.5.: Arnold tongue for asymmetric case $\tau = \pi - 0.02$. The black lines shows theoretically found border of the synchronized state. (a) Mean value of $\dot{\psi}$ on the (ν, ϵ) plane coded by color. On the right side the abrupt change (discontinuity) of the solution is visible. (b) Theoretically found Arnold tongue (black solid line) and the results of numerical simulation. The fully synchronized states obtained by numerical simulation are marked with the gray points, the synchronized states with varying phase difference (after Hopf bifurcation) are marked with the red points. The white region is desynchronized states. Only one edge of the tongue is "touching" the horizontal axis at $\Omega_* = 0.7987$.

The synchronized solution inside the tongue (Fig. 3.6 (b)) and the periodic solution for the small ν (Fig. 3.6 (a)) does not differs from the symmetric case. Moreover, the transition to synchrony by increasing the parameter ε also emerges by the infinite-period bifurcation. The typical realization of $\dot{\psi}$ close to the border is shown in Fig. 3.6 (c). The periodic solution has the property that the frequency of the oscillation of the $\dot{\psi}$, and correspondingly of ψ, is equal to the mean value of $\dot{\psi}$ (see Appendix D).

In asymmetric case the oscillator without external force has only one stable frequency (Fig. 3.2) $\Omega_* = 0.79871$. Indeed, in the Arnold tongue for this case the right edge is "detached" from the horizontal axis (see Fig. 3.5 (b)). Thus, the oscillator can be synchronized with the weak external force ($\varepsilon \ll 1$) only around the frequency Ω_*. As a result, we have asymmetric view of the Arnold tongue. However, it is not the only one asymmetry that appears. On the right side of Fig. 3.5 (a) ($\nu \gtrsim 1.2$) the discontinuity of the mean frequency value is clearly seen. It appears due to hysteretic behavior of the periodic solution. Indeed, two examples of the realization of $\dot{\psi}$ Fig. 3.6 (e) and (f) have not only different mean values, but also different period of oscillation. Slowly increasing of the parameter ε for the case with lower frequency (f) leads to abrupt jump

to the higher frequency (e), and vice versa. The hysteretic dependence of the $d\psi/dt$ on parameter ε along the dashed line ($\nu = 1.8$) in Fig. 3.6 (d) is demonstrated in Fig. 3.7 (b). The red line corresponds to increasing and the blue line to decreasing ε.

The hysteretic bistability of the periodic solution extends to the synchronized solution around the "detached" edge of the Arnold tongue. If we start on the synchronized state close to the border (Fig. 3.6 (k)) and decrease ε we will observe discontinuous transition to periodic solution with lower frequency (Fig. 3.6 (h)). Explicitly this behavior is demonstrated in Fig. 3.7 (a).

3.4. Conclusion

In this chapter we considered synchronization of an oscillator with an internal delayed feedback by an external periodic force. We found theoretically and confirmed numerically the synchronization region (the Arnold tongue) for two typical cases, with the parameter $\tau = \pi$ and $\tau = \pi - 0.02$. Since the oscillator in the first case is bistable the synchronization region has respectively two edges and symmetric form. On the contrary, in the second case, the oscillator is monostable. Therefore, the Arnold tongue for this case has asymmetric form with only one edge. However, the closeness of the parameter τ to π exhibits as a bistability, and respectively hysteresis, that appears for large frequency of the periodic force ($\nu \gtrsim 1.0$). As a result, for some values of the frequency ν and the coupling strength ε the solution of Eq. 3.3, depending on initial conditions, is not synchronized even inside the region of synchronization (Fig. 3.7 (a), the lower branch). This symmetry breaking plays crucial role for appearance of the chimeralike state (see Chapter 2).

The phase model of an oscillator with an internal delay considered in this chapter can be applied to many biological systems and laser with external feedback, where the delay can appear as natural limitation to the speed of the signals. Another possibility is when current state of the system depends on its previous states, i.e. its history. Moreover, this phase approximation can be used in systems with retarded reaction, like the systems which are already "fixed" in a certain state and controlled by an external delayed feedback. Furthermore, the problem considered in this chapter corresponds to the reaction of this system to the periodic influence. This motivates the further investigation. The border of the bistability, the change of the synchronization region in the presence of a weak noise or a small perturbation of the frequency of the external force still need to be considered.
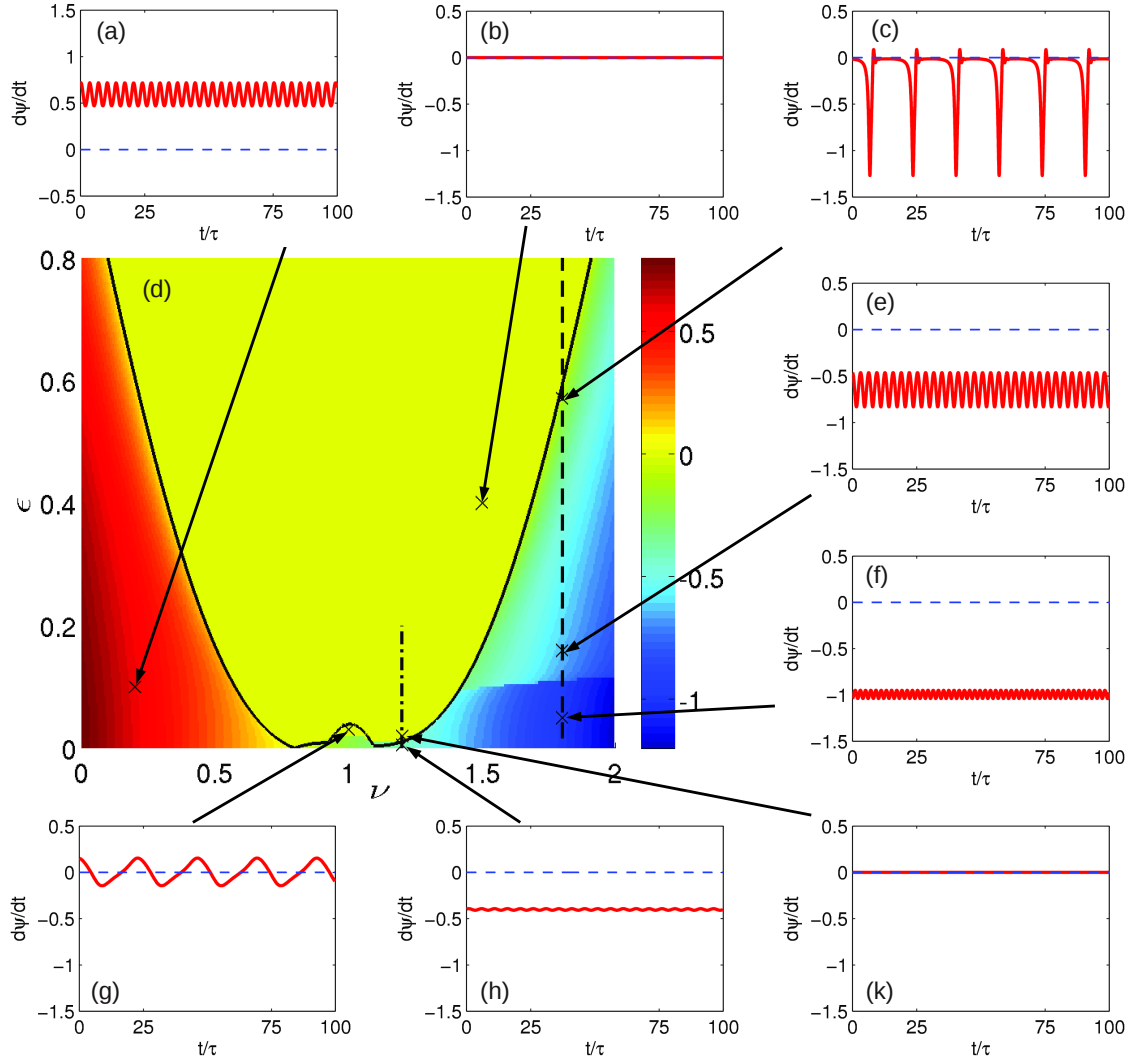
Figure 3.6.: Mean value of the $d\psi/dt$ plotted with color coding (d) on the parameters plane (ν, ε). The figures around ((a), (b),(c),(e),(f),(g),(h),(k)) show typical solutions of $d\psi/dt$ for different points on the plane pointed with arrows. Solid black line is the border of the synchronized state. Dependence of the mean frequency on ε along the black vertical dash-dotted line ($\nu = 1.2$) and dashed line ($\nu = 1.8$) are plotted in Fig. 3.7.
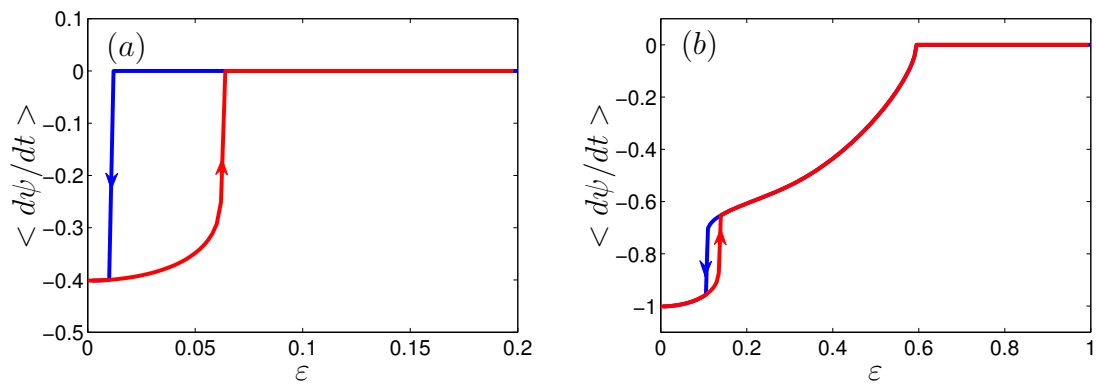
Figure 3.7.: Hysteretic behavior of the dependence of $<\dot\psi>$ on ε for (a) $\nu = 1.2$ and (b) $\nu = 1.8$ (correspond to black dash-dotted and dashed lines in Fig. 3.6). The red line and blue line are branches of increasing and decreasing ε, respectively. The horizontal plateau ($<\dot\psi> = 0$) is the synchronized solution.

4. Synchronization analysis: application to time perception

Synchronization was observed in many live systems of different scales [22, 55, 71, 80] . However, the functional role of synchrony is quite often unclear. This phenomenon can be not only vital, e.g. as a source of pacemaker in the synchronous contraction of many cells in the respiration and heart cycle [63, 11], but also be the reason of pathology, e.g. in Parkinson's disease. This phenomenon could be just presentation of a general property of self-sustained oscillators to synchrony in the presence of a weak interaction. Moreover, this property of the synchronization give an opportunity to reveal even a weak physiological influence of one system to another by using synchronization analysis. As an example of application of this analysis we discuss in this chapter the results of our work [59] on the human time perception problem.

Perception of time was always an intriguing problem. In everyday live we complete a lot of tasks which need predicting and responding in a certain time interval. This intervals could be of a wide duration range. Like a short milliseconds reaction time of our electronic equipments, several seconds spend to cross the street until the traffic light turns red, or several minutes of waiting the public transport in stations. Moreover, by usual activity, like walking, speaking, playing sports, and hearing music, we always face with the time perception task. It is a very important part of human experience. However, the underlying processes is still not completely understood.

The resent works in this field [81, 15] present the models, that propose an interaction between ability to perceive internal body signals (interoception) and the time perception. Furthermore, respiration and heart beat was suggested as a candidate to the biorhythm used in timing task [14, 45, 82, 28].

In collaboration with Olga Pollatos and Jennifer Meyer from the Psychology Department of the University of Potsdam we carried out an investigation, where we suggested the model based on the synchronization concept to find the interaction between the cardiorespiratory signals of the body and the time perception. Olga Pollatos and Jennifer Meyer performed corresponding experiments and made processing of initial data. My part of the work covered further processing of the data and a statistical analyse of the results.

This chapter we start with the discussion of time perception models and our hypothesis. Further we present the description of an experiment and the methods used to analyse obtained data by means of the synchronization concept. We then present the

results related to the synchronization analysis. The results concerning to interoceptive sensitivity we describe in Appendix E. Finally we discuss the significance of the results, correctness of our hypothesis and give suggestions for further investigations.

4.1. Time perception models

Perceptual time is not "isomorphic" to real subjective time, and many factors, like attention, working memory, ongoing activity, arousal, cognitive load, and emotional states, can be modulators of it [8]. There are many models of time estimation. Some of them assume existence of an "internal clock", with an accumulator and a pacemaker [75, 81], where an oscillator (a peacemaker) produce the sequence of pulses that are recorded in the accumulator and present the time estimation.

Recently there are another concepts which assume that perception of time is also an emotional process and depend on physiological state. The simple example when the attention and emotion affects one's time judgement is the waiting situation and being under the stress, which lead to longer time estimation. In previous models emotion and physiological states together with the cognitive functions like memory and attention were considered as a modulator of an neural clock. But in the works [15, 14, 81] the emotion and physiological state considered to function themselves as a timekeepers. According to [14] there is a direct link between the time perception and physiological processes. And our experience of time relates to emotional and visceral processes (processes in internal body organs), because they share a common neural system, namely insula cortex and the interoceptive system. It is plausible that our perception of duration is created by the rate of body signals accumulated in the insula over a given time span. Moreover, [15, 14] suggest possible relationship between heartbeat-related inputs and the perception of time. Another work [28] considered the idea that ones body rhythm is linked to the time perception, and showed that the tones preferred by the participants were in the harmonic relation (with a ratio 1:1, 3:2, and 2:1) with their individual heart rate.

To answer the questions, how internal signals like one's heartbeat could influence the time perception and what is the relationship between the time perception and internal signal processing, we used the concept of synchronization.

This relationship could be reflected in the phase locking of the internal clock with the cardiac rhythm. However, the phase locking will not increase the precision of the time estimation. Indeed, only intervals with an integer number of heartbeat will give minimal time estimation error. Whereas, for other time intervals the synchronization will lead to systematic "error". Since it was not clear how high is the effects of cardiac rhythms on the internal clock and is it enough to be measured statistically, we decided to cover a relatively wide span of time interval lengths: from 0.5 to 40 seconds.

Our main hypothesis was that heart rate does not directly determine the time esti-

mation but weakly influences it and that this effect may well depend on the interval duration [59]. Additionally, we hypothesized that interoceptive processes and inter-individual variance in interoceptive sensitivity affect the time perception accuracy.

4.2. Experimental setup

Twenty-three participants (mean age and standard deviation (M ± SD yrs) 23.8 ± 3.1; five males and eighteen females) were recruited among the students of the University of Potsdam. Using a questionnaire at the beginning of the experiment we excluded the participants with common somatic disorders and with any common psychiatric disorder. Drug use (except of contraceptives) was also an exclusion criterion. The experiments were conducted in accordance with the Declaration of Helsinki. Ethical approval from a local ethic board was obtained. All participants gave their written informed consent. The experiment was carried out in the laboratory of the Department of the Psychology of the University of Potsdam. Advanced Neuro Technology, ANT, was used as a physiological heart rate recording equipment.

The experiment was started with 10 minuts rest period. During this period baseline measurement was assessed, and individual heart rate and its average value was measured. Then the participants performed the IS task (see Appendix E), where the ability to percept the body signals, namely individual heart rate, was tested.

Afterwards, the participants performed the time interval estimation trial. We used a free reproduction task in which participants had to encode the duration of varying time intervals (so-called presentation intervals) in order to reproduce them later (so-called reproduction intervals). Every participant heard a tone with certain time length in encoding part, and asked to reproduce this given time length by pressing the button in reproduction part of the experiment. Further, we denote the beginning and end points of the presented intervals as PB and PE, respectively. Similarly, the beginning and the end points of the reproduced intervals are denoted by RB and RE. We recorded heart rate during the whole experiment. The length of the time intervals varied between 0.5 and 40 s (0.5, 2, 3, 7, 10, 14, 25, 40 s). The time reproduction task consisted of ten repetition of increasing time length (from 0.5 to 40 s) and decreasing time length (from 40 to 0.5 s) for every participant. Thus, the whole experiment lasted about 40 minutes.

4.3. Synchronization analysis

The quantity of the synchronization level is measured by the synchronization index (SI), also known as phase locking value [3, 39, 78]. This method of quantification of synchrony and interaction strength was suggested in [73, 60, 48], and it was applied to e.g. cardiorespiratory coordination [49] and brain activity [73, 60].
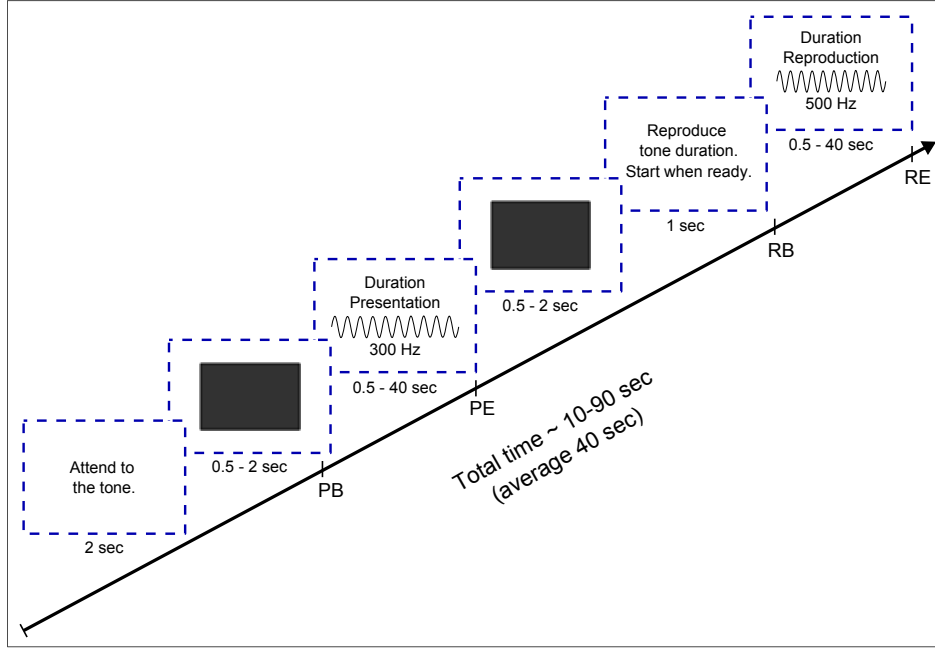
Figure 4.1.: Design of the experiment on time perception and cardiorespiratory signal processing. The participants were seated in front of a computer, where text instructions were shown on a display. The time interval was given by a tone with frequency of 300 Hz and of corresponding duration. Before the presentation begin (PB) and after the presentation end (PE) the black screen was displayed. The participants reproduced the tone by pressing the button at will, thereby indicating the reproduction begin (RB) and end (RE). During the whole experiment the ECG and respiration information were recorded.

Higher value of the synchronization index indicates a strong interdependence between oscillator's phases, i.e. synchronization. The fully synchronization is characterized by the value of SI close to one. On the contrary, in the absence of synchrony the index is nearly zero. To find the index one should first obtain the phases of oscillating processes from original data. Usually, the Hilbert transform or the complex wavelet transform and many other methods are used for this purposes [55].

To find the interdependence between the cardiac cycle and the perception of time we tested the phase of the reproduced sequence and the phase of the cardiac cycle. First, we detected all R-peaks in the electrocardiogram and labeled them by corresponding times t_k (see Fig. 4.2 a). Let's assume that the moment of pushing the button for the end of interval reproduction (reproduction end event) occurred at time τ. The phase of the R-peak preceding this event we assigned as $\phi = 0$, and the phase of the next R-peak as $\phi = 2\pi$. The times when this peaks occur we denoted as t_k and t_{k+1}. Thus, the phase of the event relative to the phase of the cardiac phase is the result of a linear interpolation (see Fig. 4.2 b) [63]:

$$\phi = 2\pi \frac{\tau - t_k}{t_{k+1} - t_k}.$$

We repeated this procedure for all N trials, and obtained a set of values ϕ_j, where
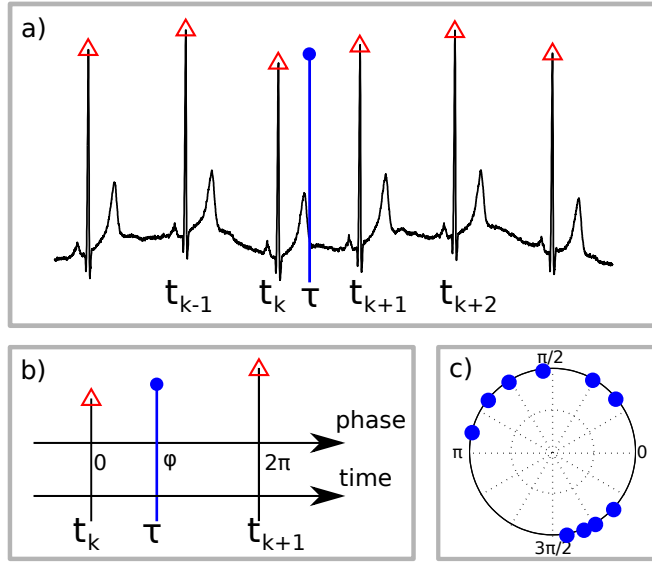
Figure 4.2.: Calculation of the phase of an event relative to the phase of cardiac cycle from [59]. (a) The black curve is ECG (electrocardiogram), the red triangles denote R-peaks, and the blue vertical circle denotes the time of the response, e.g., of reproduction begin (RB) or reproduction end (RE).(b) Defining the phase of R-peak, preceding the response, as 0 and the phase of the following R-peak as 2π we find the phase of the response ϕ by linear interpolation. (c) An example of distribution of the response phases of RE for ten different trials. From [59].

$j = 1, \ldots, N$. In Fig. 4.2 (c) we plotted this phases for one subject and certain time interval on a circle. The non uniform distribution of this phases on the circle indicates the presence of the synchronization, i.e interrelation between the processes. As it was mentioned, the quantity that measure the interrelation is the synchronization index (SI):

$$SI = \frac{1}{N} \sqrt{\left(\sum_{j=1}^{N} \cos(\phi_j) \right)^2 + \left(\sum_{j=1}^{N} \sin(\phi_j) \right)^2}. \tag{4.1}$$

We calculated synchronization indices (SIs) for every person and for the eight different interval lengths, separately for RB and RE events. Since, in the experiment we had 23 subjects, 8 time intervals, and ten repetition of the increasing and decreasing length of time intervals sequences we obtained 184 values of SI. Every index was calculated from ten trials (an example is presented in Fig. 4.2 (c)). Further, to assess the statistical significance of the obtained SI's (for each time interval and for each subject) we compared them with the index for randomly distributed points. As in the real experiment where we had (with several exceptions) 10 trials, we took 10 points randomly distributed between 0 and 2π, and calculated the synchronization index. We repeated this procedure ten thousand times. Of course, the synchronization index should tend to zeros for large number of randomly distributed points. Due to positive value of the index and the small amount of the set (10 points), we obtained the average value of the synchronization index 0.28. Also, from the random distribution we calculated

quantiles of the distribution for 0.05, 0.10, and 0.20 (see Fig. 4.3), which were used to identify significant cases (see Fig. 4.4). Finally, we checked whether the averaged synchronization indices for every time interval referring to RB and RE are significantly larger than 0.28.
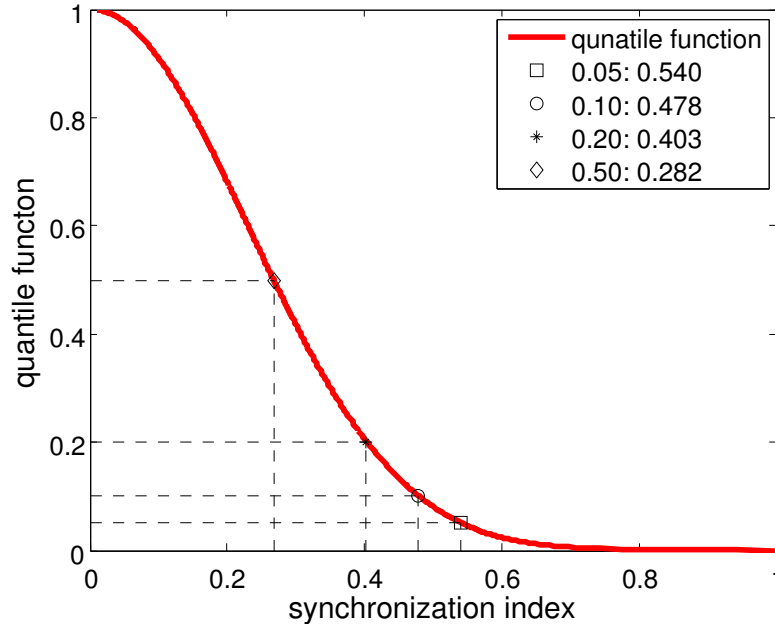

Figure 4.3.: The quantile function for synchronization index (SI) calculated from ten uniformly distributed between 0 and 2π random points. The legend shows the values of quantiles and the corresponding threshold values for SI. For example: the probability to have the value of SI larger or equal to 0.478 is 0.10. The mean value of SI 0.282 is the threshold value of the quantile 0.5.

4.4. Results

We analysed the data obtained from experiment in two phases. First, we assessed the time reproduction accuracy by comparing the time durations estimated form reproduction part with the actual time given in encoding part. Then we calculated an average absolute error score for each of the eight time intervals.

Further, we made synchronization analysis of heart beat cycle and time reproduction variables. First, we averaged SI over all subjects for every time interval referring to RB and RE (See Table 4.1). The obtained results revealed that for one time interval length in several individuals there was a tendency towards a synchronization either for reproduction begin (RB) or for reproduction end (RE). Thus, we assessed maximum synchronization index for each time interval using this indices.

For further statistical analyses we compared the obtained synchronization index (for each time interval) with the index for randomly distributed points which had an average value of 0.28 (see Methods). To test the SI obtained in experiments for significance

using t-tests, we artificially generated the distribution of indices for surrogate data. Due to multiple comparisons, for our analysis of the maximum SI we used a Bonferroni corrected significance level (i.e. statistically significance value p<.05 corresponds to $p < 0.05/8 = 0.006$; $p < 0.01$ corresponds to $p < 0.01/8 = 0.001$). Using this correction, the SIs were higher than the random distribution score for the time intervals of 3, 10, 14 and 25 seconds (see Table 4.1). We should notice that taking a maximum of SIs for RB and RE leads to slightly overestimation of the significance.

From the artificial distribution we obtained the threshold values that corresponds to 0.05, 0.10 and 0.20 quantiles. They are 0.540, 0.478 and 0.403 respectively (see Fig. 4.3). In Fig. 4.4 we show all 184 values of SI, and also the threshold values depicted as horizontal lines. The number of cases when the SI's were larger than threshold values are presented in Table 4.2.

Table 4.1.: Statistical analysis of the synchronization indices (SI) for different time intervals (Δt): The mean values of SI are averaged over 23 participants. Each synchronization index was computed from 10 measurements, obtained from 10 trials. The fourth column shows the mean of the maximal(from RB and RE) index. Notations for the significance level: *p < 0.05; **p < 0.01; n.s. stands for not significant

Δt, sec	RB	RE	Max. SI		
	Mean SI (SD)	Mean SI (SD)	Mean SI (SD)	T(df=23)	p
0.5	0.30 (0.14)	0.27 (0.11)	0.34 (0.12)	2.59	n.s
2	0.25 (0.13)	0.28 (0.15)	0.36 (0.14)	1.76	n.s
3	0.30 (0.15)	0.28 (0.14)	0.38 (0.12)	4.03	*
7	0.25 (0.12)	0.26 (0.15)	0.34 (0.12)	2.53	n.s
10	0.30 (0.17)	0.30 (0.17)	0.38 (0.14)	3.63	*
14	0.25 (0.13)	0.30 (0.16)	0.36 (0.14)	2.94	*
25	0.27 (0.13)	0.34 (0.15)	0.39 (0.13)	4.23	**
40	0.30 (0.15)	0.28 (0.16)	0.36 (0.16)	2.65	n.s

Table 4.2.: The number of cases N_q when synchronization index (SI) was larger than threshold values, obtained for random distributed points on a circle (see Fig. 4.4) for different time intervals Δt and for reproduction begin (RB) and reproduction end (RE) event points.

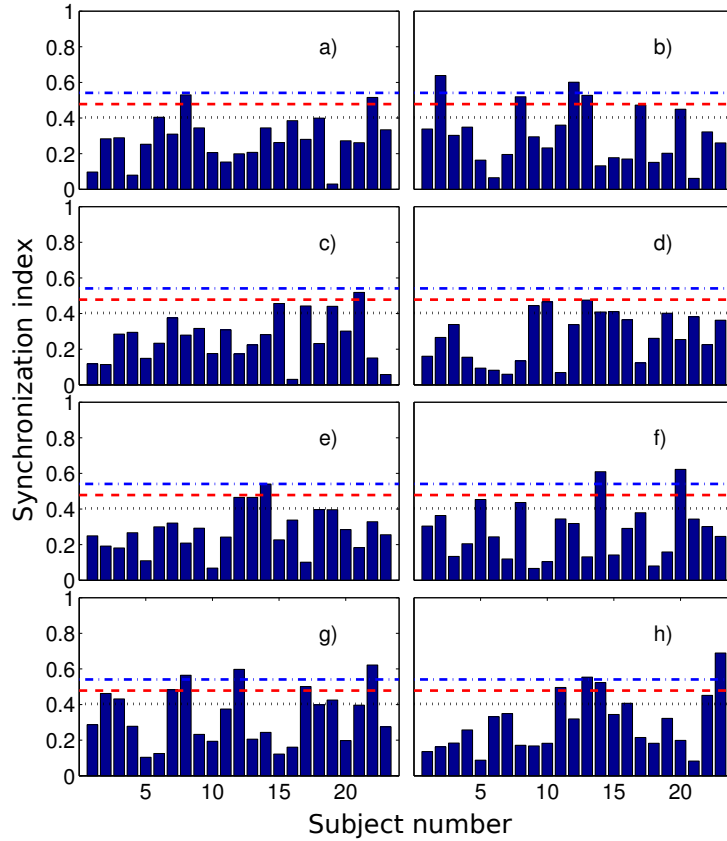| Δt, sec	RB			RE		
	$N_{0.05}$	$N_{0.10}$	$N_{0.20}$	$N_{0.05}$	$N_{0.10}$	$N_{0.20}$
0.5	1	1	2	0	2	3
2	0	1	3	2	4	6
3	2	2	3	0	1	4
7	1	1	2	0	0	5
10	4	5	5	1	1	3
14	1	1	2	2	2	4
25	1	1	4	3	5	8
40	1	4	6	2	4	6

Figure 4.4.: The synchronization indices of RE response for all 23 participants and for different interval durations. Horizontal blue dash-dotted line, red dashed line, and black dotted line show 5%, 10%, and 20% quantile thresholds, with the values of 0.540, 0.478 and 0.403, correspondingly. Interval durations are 0.5s (a),2s (b), 3s (c), 7s (d), 10s(e), 14s(f),25s (g), and 40s (h). From [59].

From Fig. 4.4 and Table 4.2 one can see that for time interval 25 s and for RE event, 3,5, and 8 subjects out of 23 reached significance level of 5%, 10%, and 20% quantile, correspondingly. RE event for time intervals 2 and 40 seconds is also characterized by high SI (6 out of 23 for 20% quantile).

Further, we estimate the significance of the synchronization analysis by means of statistical analysis. We compared our results (in Table 4.2) with an amount of cases obtained in a random distribution model. We used the following formula of the probability to have n events with the probability q within N measurements

$$P(n,q) = C_N^n (1-q)^{(N-q)} q^n, \tag{4.2}$$

where C_N^n is the binomial coefficient. In Fig.4.5 lines show the probabilities $P(n,q)$ for $q = 0.05$, $q = 0.10$, and $q = 0.20$ for $N = 23$ measurements for each of eight time intervals, and symbols (circles and tiangles) depict the values of N_q actually obtained for these quantiles (see Table 4.2). If these symbols are situated close to the maxima of the probability curves it means that the results are indistinguishable from the random
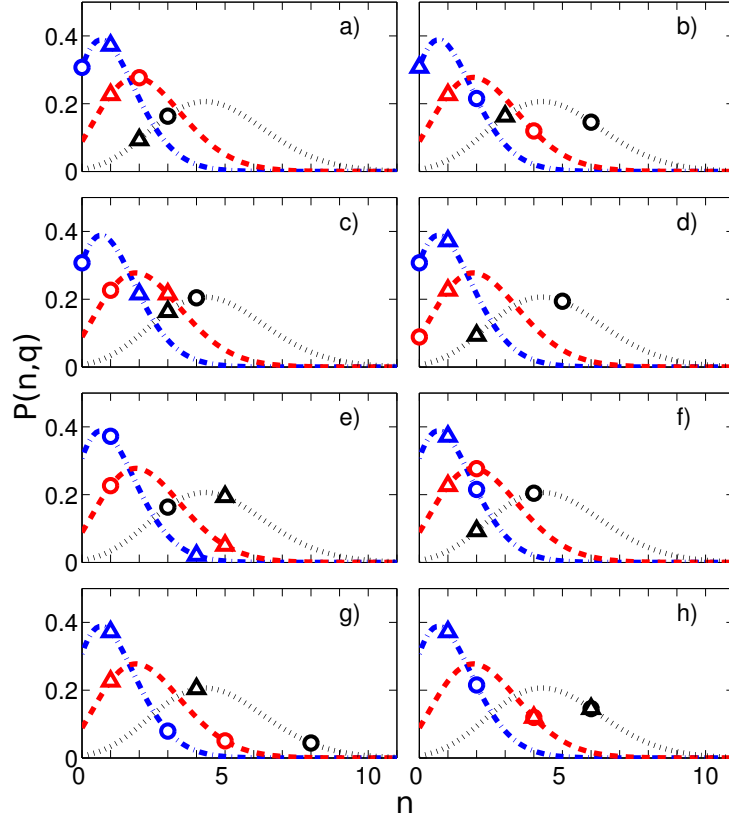
Figure 4.5.: Probability to have n cases with probability q within N measurements (see Eq. 4.2)for different interval durations: 0.5s (a),2s (b), 3s (c), 7s (d), 10s(e), 14s(f), 25s (g), and 40s (h). The blue dash-doted, red dashed, and black dotted lines correspond to the probability $q = 0.05$, $q = 0.1$, and $q = 0.2$. The experimentally obtained values of N_q (see Table 4.2) and corresponding probabilities are shown by triangles (for reproduction begin) and circles (for reproduction end). The total number of measurements for each time interval is $N = 23$. From [59].

distribution and thus non-significant. On the contrary, if the symbols are positioned on the tail of the distribution, then the indices are larger than can be expected for the random distribution. The difference from the random case is especially pronounced for the RE events for 25s interval.

Finally, we performed correlation analyses between synchronization indices and a. corresponding time reproduction accuracy and b. interoceptive sensitivity (IS) (see Appendix E). Time reproduction accuracy was not significantly correlated with any corresponding synchronization index (maximum SI used). However, we found significant correlation between IS and maximum SI for 2s time intervals ($r = 0.54$, $p < 0.05$, p-value Bonferroni corrected; see Fig. E.1).

4.5. Discussion

The results show that the cardiac rhythm affects time perception. By using synchronization analysis we observed that the cardiac cycle influences the encoding and reproduction of time. For time intervals of 3, 10, 14 and 25 seconds in the whole sample the average SI's between reproduction start/stop points and heart cycle were marginally significant in comparison to the random distribution of points on a circle. However, on average, we did not observe a significant synchronization between heart rate and time reproduction responses for intervals of shorter as well as of longer duration. In contrast, for individual persons we observed significant synchrony for intervals of 2 and 25 seconds length.

We hypothesized that the interaction and synchronization between heart beat and time preproduction is more possible when the intervals cover at least 3 and up to 30 heart cycles. The measurements of during the baseline show that mean heart rate was 66 beats per minute (bpm). However, individual heart rates varied between participants from 49 bpm to 84 bpm. Thus, the intervals between 3 second and 25 seconds were within this preferable time length, and therefor were with higher SI's. To specify it, the future studies should include on line individual heart rate assessment and interval length adjustment.

The hight variance of the heart rate between participants imply that significant synchronization can be found on an individual level and only for certain time length. To find it we used two other measures that take into account an inter-individual variety, namely vagal control and interoceptive sensitivity (IS)(see Appendix E).

We obtained a significant positive correlation between IS and the maximum of SI for 2 s time interval. This means that the participants with higher IS show higher phase locking between heart cycle and time reproduction star/stop responses. In the work [45] it was demonstrated that IS is associated with time reproduction accuracy in the multi-second range. Our results show that we have synchronization for the shorter time range of 2 s. It is need to be noticed, that this time interval was only one interval with significantly many individual high SIs.

The hypothesis that the higher degree of synchronization lead to higher time reproduction accuracy was not conformed by the results. We did not observe significant correlation between SI and time reproduction accuracy. Therefore our hypothesis that heart rate only influences the perception of time and not determine it found evidence. Indeed, if we would have the phase locked synchronization, then the reproduction accuracy would be high only for time intervals which is the whole multiple to the individual heart cycle. Alternatively, if the time interval is not rational to the heart cycle then the reproduction error would be high. Thus, high synchronization degree could be the source of "errors" in timing tasks as e.g. demonstrated by [28]. The latter study could showed a harmonic relation (1:1, 3:2, 2:1) between the participant's individual heart rates and the tempo of represented successive tones. This support our idea that one's own cardiac rhythm is used in a timing task.

At the end some shortcomings have to be noticed. In our study we had rather small sample size, wide range of time length, which caused to make less repetitions. The next studies with more repetitions and with more participants as well as a new experimental design with online heart rate assessment and interval duration adjustment could help to clarify our assumptions. Also focusing on intervals between 2,3 s and 25 s and using another biorhythm like respiration should be included in future works.

5. Conclusion

Synchronization has wide range of application in modern researches. In this work, the modeling of complex regimes of synchronization, such like chimera state, and application of the synchronization analysis in time perception model were considered.

In chapter 2 it was shown, that minimal generalization of the model of globally coupled identical oscillators can lead to complex solutions like chimera state. Initially homogeneous system of oscillators with intrinsic delayed feedback splits into two domains with different dynamics: the mutually synchronized coherent cluster and the desynchronized cloud. The synchronized part of the system has nearly constant frequency, whereas the oscillators in the cloud demonstrate chaotic behaviour with the strongly fluctuating instantaneous frequency. The emergence of the chimeralike state was explained by *dynamically sustained bistability*. The global coupling make the oscillators effectively bistable, and this symmetry breaking slits them into two groups. The mean field created by two domains, on the one hand, stabilize the coherent part, and on the other hand, does not let this part grow by capturing other oscillators from the incoherent part.

It was also shown, that chimeralike state can be obtained in a system, where individual oscillators are naturally amplitude and/or frequency bistable. In two presented examples the phase shift between the mean field and the phase of oscillator is frequency dependent. Delay in the coupling or frequency of the external linear circuit were "adjusted" in such a way, that the coupling affects repulsively to the oscillators in one of the bistable state, and attractively to the oscillators in other state.

The role of bistability of the phase oscillator with intrinsic delayed feedback to create the chimeralike state was considered in chapter 3. The theoretical analysis of synchronization of the oscillator by external periodic force revealed non-typical Arnold tongues for bistable and nearly bistable regimes. Emergence of complex states, like chimeralike state, was explained by asymmetric and hysteretic behaviour of the Arnold tongue in large frequency part for the oscillator in nearly bistable state.

Synchronization analysis can be used to revel an interaction or interdependence between elements of a complex system. In the third part of this dissertation (in chapter 4), we presented results of the collaborative work, where we used the synchronization analysis to find influence of the cardiac rhythm to human perception of time in the time interval reproduction task. Our approach was based on synchronization of two weak interacting phase oscillators. Using the techniques of experimental studies of synchronization we reconstructed the phase of an irregular oscillation, like human heartbeat, and made

statistical analysis to qualify the interaction strength by means of the synchronization index.

The results show that in comparison to random distribution the synchronization index in the whole sample was marginally significant for time intervals of 3, 10, 14, and 25 seconds. And in the individual level significant synchrony was observed for 2 and 25 second intervals. According to the assumption, that high time interval reproduction accuracy related to the ability of a person to percept her/his own body signals, which is characterised by the interoseptive sensitivity, we observed positive correlation between the interospetive sensitivity and the synchronization index for 2 second time intervals.

We concluded that the heart cycle signals can be used as input signals to judge the reproduced time intervals in the range of several seconds. Moreover, oscillating processes like heartbeat and respiration can be interpreted as an inflow units in the time perception mechanism.

The results of this work can help to explains the emergence of the complex regimes, like chimera states in many systems. The recent works show that chimera states appears in chemical oscillations, and in opto-electronic lasers, and networks. And we hope that the result of this research can support future development of other applications in this fields.

This work is interesting not only for solution of the fundamental theoretical problems, but also can find a practical application in modern branches of science. Hereby, the findings of this work can be applicable in neurodynamics. For example, unihemispheric sleeping, the possibility of animals to sleep with one part of their brain when another part is awake, can quite possibly be explained by the chimera state. Or in contrary, understanding of the emergence of the complex synchronization regimes can be used to prevent and recognise undesirable synchrony onsets, that lead to a pathology, e.g. to Parkinson decease.

Moreover, this work demonstrates that considering a synchronization of complex models extends our understanding of difficult processes such as time perception of human and animals. Confirmation of the assumption, that the ability of the person to perceive ongoing body signals affect their time sensing, support a new model of interaction between physiological states and emotions. It can add new area of research in this field and suggest directions of the future investigations.

This research provide ample opportunity for scientists to work in interdisciplinary projects, that can incorporate different branches of the science, like physics, physiology, psychology, biology, and neuroscience.

A. The perturbation equations for the cluster and the cloud

To show the stability of the cluster (stability of synchronized state in the cluster) and unstablility of the cloud (unstability of synchronized state in the cloud) we use Lyapunov exponents, which will be found from linearized equations.

Let's assume that we have n oscillators in the cluster and m oscillators in non synchronized "cloud". Then we rewrite the sum in the global coupling in Eq. 2.5 as following

$$
\begin{aligned}
\sum_{j=1}^{n+m} &\sin(\phi_j(t) - \phi_k(t) + \beta) = \\
&= \sum_{j=1}^{n+m} [\sin(\phi_j(t) + \beta)\cos(\phi_k(t)) - \cos(\phi_j(t) + \beta)\sin(\phi_k(t))] = \\
&= n\sin(\Phi(t) + \beta)\cos(\phi_k(t)) - n\cos(\Phi(t) + \beta)\sin(\phi_k(t)) + \\
&+ \underbrace{\sum_{j=n+1}^{n+m} \sin(\phi_j(t) + \beta)\cos(\phi_k(t))}_{A(t)} - \underbrace{\sum_{j=n+1}^{n+m} \cos(\phi_j(t) + \beta)\sin(\phi_k(t))}_{B(t)}.
\end{aligned}
\tag{A.1}
$$

where $\Phi(t)$ is the phase of the cluster.

So the equation for individual oscillator will be

$$
\begin{aligned}
\dot{\phi}_k(t) = \ & 1 + \alpha\sin(\phi_k(t-\tau) - \phi_k(t)) + \\
&+ \tfrac{\epsilon n}{n+m}[\sin(\Phi(t) + \beta)\cos(\phi_k(t)) - \cos(\Phi(t) + \beta)\sin(\phi_k(t))] + \\
&+ \tfrac{\epsilon}{n+m}[A(t)\cos(\phi_k(t)) - B(t)\sin(\phi_k(t))].
\end{aligned}
\tag{A.2}
$$

Let's take this equation for the oscillator which has the solution close to the cluster's and linearize it around the cluster solution. Our aim is to show that this solution is stable.

$$
\begin{aligned}
\dot{\delta}(t) = \ & \alpha\cos(\Phi(t-\tau) - \Phi(t))(\delta_\tau - \delta) - \\
&- \tfrac{\epsilon n}{n+m}\underbrace{[\sin(\Phi(t) + \beta)\sin(\Phi(t)) + \cos(\Phi(t) + \beta)\cos(\Phi(t))]}_{\cos(\beta)}\delta - \\
&- \tfrac{\epsilon}{n+m}[A(t)\sin(\Phi(t)) + B(t)\cos(\Phi(t))]\delta = \\
= \ & \alpha\cos(\Phi(t-\tau) - \Phi(t))(\delta_\tau - \delta) - \\
&- \underbrace{\frac{\epsilon}{n+m}[n\cos(\beta) + A(t)\sin(\Phi(t)) + B(t)\cos(\Phi(t))]\delta}_{X(t)}.
\end{aligned}
\tag{A.3}
$$

If we set the definition of $A(t)$, $B(t)$ to the last equation then we obtain simple equation for δ (see Eq. 2.8):

$$
\begin{aligned}
\dot{\delta}(t) = \ & \alpha \cos(\Phi(t-\tau) - \Phi(t))(\delta_\tau - \delta) - \\
& - \left[\frac{\epsilon n}{n+m} \cos(\beta) + \frac{\epsilon}{n+m} \sum_{j=n+1}^{n+m} \cos(\phi_j(t) - \Phi(t) + \beta) \right] \delta.
\end{aligned}
\tag{A.4}
$$

In the same way we can find the Lyapunov exponents for an oscillator of the cloud.

Here we observe phase difference of two oscillators from the cloud. First, we write equation for them in similar way like in (A.2):

$$
\begin{cases}
\dot{\phi}_1(t) = \ & 1 + \alpha \sin(\phi_1(t-\tau) - \phi_1(t)) + \\
& + \frac{\epsilon n}{n+m} \left[\sin(\Phi(t) + \beta) \cos(\phi_1(t)) - \cos(\Phi(t) + \beta) \sin(\phi_1(t)) \right] + \\
& + \frac{\epsilon}{n+m} \left[A(t) \cos(\phi_1(t)) - B(t) \sin(\phi_1(t)) \right] \\
\dot{\phi}_2(t) = \ & 1 + \alpha \sin(\phi_2(t-\tau) - \phi_2(t)) + \\
& + \frac{\epsilon n}{n+m} \left[\sin(\Phi(t) + \beta) \cos(\phi_2(t)) - \cos(\Phi(t) + \beta) \sin(\phi_2(t)) \right] + \\
& + \frac{\epsilon}{n+m} \left[A(t) \cos(\phi_2(t)) - B(t) \sin(\phi_2(t)) \right].
\end{cases}
\tag{A.5}
$$

Let's define the difference of the phases as $\Delta = \phi_1 - \phi_2$. The equation for Δ

$$
\begin{aligned}
\dot{\phi}_1(t) - \dot{\phi}_2(t) = \dot{\Delta}(t) = \ & \alpha(\sin(\phi_1(t-\tau) - \phi_1(t)) - \sin(\phi_2(t-\tau) - \phi_2(t))) + \\
& + \frac{\epsilon n}{n+m} \sin(\Phi(t) + \beta)(\cos(\phi_1(t)) - \cos(\phi_2(t))) - \\
& - \frac{\epsilon n}{n+m} \cos(\Phi(t) + \beta)(\sin(\phi_1(t)) - \sin(\phi_2(t))) + \\
& + \frac{\epsilon}{n+m} A(t)(\cos(\phi_1(t)) - \cos(\phi_2(t))) - \\
& - \frac{\epsilon}{n+m} B(t)(\sin(\phi_1(t)) - \sin(\phi_2(t))).
\end{aligned}
\tag{A.6}
$$

We assume that two oscillators are close to each other, i.e. $\Delta << 1$ and $\phi_1 \approx \phi_2 \approx \phi$. Further, we linearize the previous equation therm by therm.

The first therm:

$$
\sin(\phi_1(t-\tau) - \phi_1(t)) - \sin(\phi_2(t-\tau) - \phi_2(t)) = 2\cos(\phi_\tau - \phi)\sin\left(\frac{\Delta_\tau - \Delta}{2}\right) \approx
$$

$$
\approx \cos(\phi_\tau - \phi)(\Delta_\tau - \Delta).
$$

Difference of the sine and cosine:

$$
\sin(\phi_1(t)) - \sin(\phi_2(t)) = 2\cos(\phi)\sin(\Delta/2) \approx \cos(\phi)\Delta.
$$

$$
\cos(\phi_1(t)) - \cos(\phi_2(t)) = -2\sin(\phi)\sin(\Delta/2) \approx -\sin(\phi)\Delta.
$$

So the equation for Δ

$$
\begin{aligned}
\dot{\Delta}(t) = \ & \alpha \cos(\phi_\tau - \phi)(\Delta_\tau - \Delta) - \\
& - \frac{\epsilon n}{n+m} \sin(\Phi(t) + \beta)\sin(\phi)\Delta - \frac{\epsilon n}{n+m} \cos(\Phi(t) + \beta)\cos(\phi)\Delta - \\
& - \frac{\epsilon}{n+m} A(t)\sin(\phi)\Delta - \frac{\epsilon}{n+m} B(t)\cos(\phi)\Delta.
\end{aligned}
\tag{A.7}
$$

43

Or if we collect therms with Δ and Δ_τ

$$
\begin{aligned}
\dot{\Delta}(t) = \ & \alpha \cos(\phi_\tau - \phi)\Delta_\tau - \\
& -\alpha \cos(\phi_\tau - \phi)\Delta - \\
& - \left[\tfrac{\epsilon n}{n+m} \sin(\Phi(t) + \beta) \sin(\phi) + \tfrac{\epsilon n}{n+m} \cos(\Phi(t) + \beta) \cos(\phi) + \right. \\
& \left. + \tfrac{\epsilon}{n+m} A(t) \sin(\phi) + \tfrac{\epsilon}{n+m} B(t) \cos(\phi) \right] \Delta.
\end{aligned}
\tag{A.8}
$$

If we use the definition of $A(t)$, $B(t)$ and $\Phi(t)$, we have simple equation for Δ (see Eq. 2.9)

$$
\begin{aligned}
\dot{\Delta}(t) = \ & \alpha \cos(\phi_\tau - \phi)(\Delta_\tau - \Delta) - \\
& - \left[\tfrac{\epsilon n}{n+m} \cos(\Phi - \phi + \beta)\Delta - \tfrac{\epsilon}{n+m} \sum_{j=n+1}^{n+m} \cos(\phi_j - \phi + \beta) \right] \Delta.
\end{aligned}
$$

$$
\dot{\Delta}(t) = \alpha \cos(\phi_\tau - \phi)(\Delta_\tau - \Delta) - \frac{\epsilon}{n+m} \sum_{j=1}^{n+m} \cos(\phi_j - \phi + \beta)\Delta.
\tag{A.9}
$$

Eqs. (A.9) and (A.4) are similar linear delay differential equations, which can be written as (compare with Eq. 2.7)

$$
\dot{\delta} = a(t)\delta_\tau - (a(t) + b(t))\delta.
\tag{A.10}
$$

where

$$
a(t) = \alpha \cos(\phi(t - \tau) - \phi(t)),
$$

$$
b(t) = \frac{\epsilon}{n+m} \sum_{j=1}^{n+m} \cos(\phi_j - \phi + \beta).
$$

B. Stability analysis of a linear delay differential equation

As it was shown in Section 2.5 stability of the fully synchronized state, and in the Section 3.2 the problem of synchronization of an oscillator with internal delayed feedback loop by external periodic force (Eq. 3.1) lead to the linear delay differential equation of the following form

$$\dot{\delta} = a\delta_\tau - (a + b)\delta. \tag{B.1}$$

This equation is similar to the Hayes equation [26], the simplest example of linear delay differential equation. The difference of Eq. B.1 from Hayes equation is another combination of parameters in scalar ODE part. In this section we consider the stability region of the zero solution of Eq. B.1 .

Stability analysis starts with the characteristic function $D(\lambda)$. For Eq. B.1 it is

$$D(\lambda) = \lambda + a + b - ae^{-\lambda\tau}. \tag{B.2}$$

The solutions of the characteristic equation

$$D(\lambda) = \lambda + a + b - ae^{-\lambda\tau} = 0, \tag{B.3}$$

gives us characteristic exponents. In general, this equation has infinite many solutions.

One can find the exact solution by means of the Lambert function [38],[13], which is defined as the function satisfying

$$W(z)e^{W(z)} = z,$$

where W is a complex function.

Multiplying the characteristic equation Eq. B.3 by τ and defining a new variable $z = \lambda\tau$ we have

$$z = Ae^{-z} - A - B, \tag{B.4}$$

where $A = a\tau$, $B = b\tau$. Then, the solution by the Lambert function is

$$z = W(Ae^{A+B}) - A - B.$$

The solution is stable if z is negative, and it happens if only if

$$Re(W_0(Ae^{A+B})) - Re(A + B) < 0,$$

where $W_0(\cdot)$ is the zero branch of the Lambert W function [67]. Finding the stability chart by this method is possible only numerically.

We find stability chart analytically, by D-subdivision method [27]. Therefor, we search for the values of the parameters when the real parts of some characteristic exponents λ change the sign. This set of parameters give us the curves (D-curves) in the parameters plane.

Since we are interested in real parts of the characteristic exponents we make a substitution $\lambda = \gamma \pm i\omega$, $\omega > 0$ in characteristic equation $D(\lambda) = 0$ and separate real and imaginary parts. It gives

$$Re: \ \gamma + a + b - ae^{-\gamma\tau}\cos(\omega\tau) = 0,$$
$$Im: \ \omega + ae^{-\gamma\tau}\sin(\omega\tau) = 0.$$

One can find D-curves as a parametric function of ω by the condition $\gamma = 0$.

$$Re: \ a + b - a\cos(\omega\tau) = 0,$$
$$Im: \ \omega + a\sin(\omega\tau) = 0.$$

Here we have two set of solutions. The first, if $\omega\tau \neq k\pi$, then

$$a = -\frac{\omega}{\sin(\omega\tau)}, \ b = a(\cos(\omega\tau) - 1) = \frac{\omega(1 - \cos(\omega\tau))}{\sin(\omega\tau)} = \omega\tan(\omega\tau/2). \tag{B.5}$$

and the second,

$$a = -1/\tau, \ b = 0; \text{ and } b = 0 \text{ as a curve}, \tag{B.6}$$

if $\omega = 0$.

Along this curves γ changes it's sign by crossing imaginary axes. In order to find how, we take partial derivative of $D(\lambda)$ with respect to one parameter. Let's take parameter b:

$$\gamma_b' + 1 - a(-\tau\cos(\omega\tau)\gamma_b' - \tau\sin(\omega\tau)\omega_b') = 0,$$
$$\omega_b' + a(-\tau\sin(\omega\tau)\gamma_b' + \tau\cos(\omega\tau)\omega_b') = 0,$$

where we denoted with γ_b' and ω_b' partial derivatives of γ and ω with respect to parameter b. After some rearrangements we obtain the system of linear equations with respect to γ_b' and ω_b':

$$(1 + a\tau\cos(\omega\tau))\gamma_b' + a\tau\sin(\omega\tau)\omega_b' = -1,$$
$$-a\tau\sin(\omega\tau)\gamma_b' + (1 + a\tau\cos(\omega\tau))\omega_b' = 0.$$

The solution for γ_b' is

$$\gamma_b' = \frac{-(1 + a\tau\cos(\omega\tau))}{(1 + a\tau\cos(\omega\tau))^2 + (a\tau\sin(\omega\tau))^2}. \tag{B.7}$$

Let's find the sign of γ_b' along the D-curves. If $\omega = 0$, then from Eq. B.6 and B.7 $\gamma_b' = -(1+a\tau)^{-1}$. If $a > -1/\tau$ then $\gamma_b' < 0$, i.e. the critical exponent crosses imaginary

axes from right to left when b increases, so unstable characteristic exponents become stable. Otherwise, if $a < -1/\tau$, then critical exponent crosses imaginary axes from left to right when b increases, i.e becomes unstable.

For other D-curves defined by Eq. B.5 the equation B.7 turns to

$$\gamma'_b = \frac{-(1 - \omega\tau\cos(\omega\tau)/\sin(\omega\tau))}{(1 + \omega\tau\cos(\omega\tau)/\sin(\omega\tau))^2 + (\omega\tau)^2} =$$

$$= \frac{\frac{\omega\tau}{\tan(\omega\tau)} - 1}{\left(\frac{\omega\tau}{\tan(\omega\tau)} - 1\right)^2 + (\omega\tau)^2}.$$

The delimiter is always positive, so $\text{sign}(\gamma'_b) = f(\omega\tau) = \text{sign}((\omega\tau)/\tan(\omega\tau) - 1)$. This function with corresponding curves in the (a, b) plane is shown in the Fig. B.1. The red and blue lines are positive and negative sign of γ'_b correspondingly. As it was mentioned before, if γ'_b is negative along some certain line, then real part of two complex conjugate characteristic exponents become negative, i.e. stable, when the line is crossed in the b increasing direction. In contrary, if γ'_b is positive, crossing the line in b increasing direction makes real value of two complex conjugate exponents become positive, i.e. unstable.

One can also use Stepan's formula [68, 27] to find number of unstable characteristic exponents. They are shown in the right plot of Fig. B.1. So the stable region is that with 0 unstable characteristic exponents. Separately the stable region for zero solution of the Eq. B.1 is shown in Fig. 3.3.
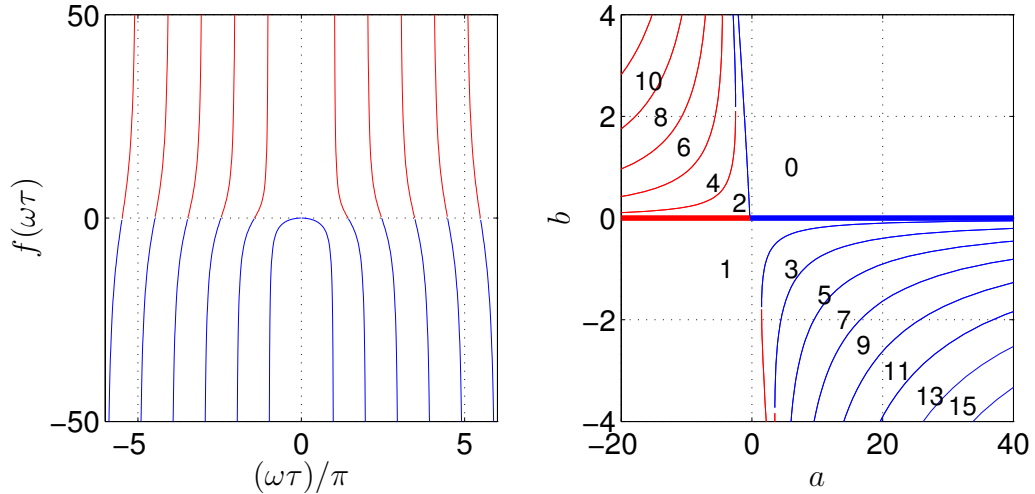

Figure B.1.: In the left figure the function $f(\omega\tau) = (\omega\tau)/\tan(\omega\tau) - 1$ and in the right figure the D-curves are shown. The positive and negative values of the γ'_b shown with the red and blue color lines correspondingly. Every crossing of the red (blue) lines in the directing of growing b increases (decreases) the number of unstable characteristic exponents for bold line to one, and for thin lines to two. The numbers in the (a, b) planes show the number of unstable characteristic exponents.

C. Hopf bifurcation curve

The Hopf bifurcation curve for the linear delay differential equation B.1 on the parametric plane (a, b) is given as

$$a(\omega) = -\frac{\omega}{\sin(\omega\tau)}, \ b(\omega) = \omega\tan(\omega\tau/2),$$

where $\omega \in [0, 1]$ (see Fig. 3.3).

If the parameter $\alpha \geq 1/\tau$ in Eq. 3.2 , then at some values of the parameter ν the coefficient a of Eq. B.1 will be on the left side of the bifurcation curve, i.e. in the unstable region. The critical (boundary) values are obtained form the condition of equality $a = \alpha\cos(\nu_{cr}\tau) = 1/\tau$:

$$\nu_{cr1} = \frac{\arccos(-1/(\alpha\tau))}{\tau}, \ \nu_{cr2} = \frac{2\pi - \arccos(-1/(\alpha\tau))}{\tau}.$$

Let's assume that

$$\nu \in \left[\nu_{cr1}, \nu_{cr2}\right],$$

then for given ν the bifurcation curve is crossed at (a_*, b_*), where

$$a_* = \alpha\cos(\nu\tau) = -\frac{\omega(\nu)}{\sin(\omega(\nu)\tau)}. \tag{C.1}$$

and

$$b_* = \varepsilon\cos(\psi_0) = -\frac{\omega(\nu)}{\sin(\omega(\nu)\tau)}. \tag{C.2}$$

Form Eq. C.1 we can find transcendental equation for $\omega(\nu)$

$$\omega(\nu) + \alpha\cos(\nu\tau)\sin(\omega(\nu)\tau) = 0.$$

To solve this equation we should know the domain of ω. The minimal value is zero, and the maximal value ω_{max} is defined by the condition $min(a) = -\alpha$:

$$-\alpha = -\frac{\omega_{max}}{\sin(\omega_{max}\tau)},$$

$$\omega_{max} - \alpha\sin(\omega_{max}\tau) = 0.$$

To stay in the stability region the value of b should be larger that b_*. Thus, from Eq. C.2

$$\varepsilon \cos(\psi_0) \geq -\frac{\omega(\nu)}{\sin(\omega(\nu)\tau)}.$$

We substitute the value of $\varepsilon \cos(\psi_0)$ using Eq. 3.7

$$\sqrt{\varepsilon^2 - (\nu + \alpha \sin(\nu\tau) - 1)^2} \geq -\left(\omega(\nu)\tan\left(\frac{\omega(\nu)\tau}{2}\right)\right),$$

finally we have the condition for ε

$$\varepsilon > \sqrt{\left(\omega(\nu)\tan\left(\frac{\omega(\nu)\tau}{2}\right)\right)^2 + (\nu + \alpha \sin(\nu\tau) - 1)^2}.$$

D. Periodic solution

Here we introduce a periodic solution for Eq. 3.2. Let's consider that the Eq. 3.2 has the periodic solution with period T:

$$\psi(t+T) = \psi(t), \ \dot{\psi}(t+T) = \dot{\psi}(t).$$

We denote the mean value of the frequency as Ω, thus

$$\dot{\psi} = \Omega + f(t),$$

where $f(t)$ is a periodic function with zero mean value:

$$f(t+T) = f(t), \ \int_0^T f(s)ds = 0.$$

Th phase at arbitrary time t is then

$$\psi = \Omega t + \int_{t_0}^t f(s)ds,$$

and if we apply it to Eq. 3.2

$$\dot{\psi}(t) = 1 - \nu + \alpha \sin\left(\Omega(t-\tau) + \int_0^{t-\tau} f(s)ds + \psi_0 - \Omega t - \int_0^t f(s)ds - \psi_0 - \nu\tau\right)$$

$$-\epsilon \sin\left(\Omega t + \int_0^t f(s)ds + \psi_0\right) =$$

$$= 1 - \nu - \alpha \sin\left(\Omega\tau + \nu\tau + \int_{t-\tau}^t f(s)ds\right) - \epsilon \sin\left(\Omega t + \int_0^t f(s)ds + \psi_0\right).$$

Similarly we can write it the for time $t+T$

$$\dot{\psi}(t+T) = 1 - \nu - \alpha \sin\left(\Omega\tau + \nu\tau + \int_{t+T-\tau}^{t+T} f(s)ds\right) - \epsilon \sin\left(\Omega t + \Omega T + \int_0^{t+T} f(s)ds + \psi_0\right).$$

If we take into account the periodicity of $f(t)$ and that the mean of $f(t)$ is zero:

$$\dot{\psi}(t+T) = 1 - \nu - \alpha \sin\left(\Omega\tau + \nu\tau + \int_{t-\tau}^t f(s)ds\right) - \epsilon \sin\left(\Omega t + \Omega T + \int_0^t f(s)ds + \psi_0\right).$$

If we compare the results for $\dot{\psi}(t)$ and for $\dot{\psi}(t+T)$ we see that $\Omega T = 2\pi k, \ k \in N$. It means that, due to the periodicity, $\dot{\psi}$ oscillates exactly with the frequency equal to the mean value of it.

E. Individual sensitivity to body signals and heart rate variability

In this chapter we present the results published in [59], but not presented in Chapter 4. It is mostly relate to measuring of an individual difference of perception of body signals, like one's heart beat or respiration.

Ability of a person to perceive a body reaction, so called interoception, significantly differs. It is associated with emotion: the feeling of an emotion happened because of our perception of body signals [30, 77, 29, 18]. One of the measures of an individual's sensitivity is *interoceptive sensitivity* (IS), which is often used as a quantity of an ability to perceive one's heartbeats [16, 57]. Individuals with higher sensitivity (IS) should intensively experience emotions. Several works conformed this prediction [58, 56].

The time perception model proposed by Craig and Wittmann [15, 14, 81] suppose an interaction between interoceptive process and time perception: the emotional and visceral states is reflected in the insular cortex and form our experience of time.

E.1. Measurement of IS

To measure interoseptive sensitivity (IS) the participants of the experiment completed following task: They were asked to count their own heartbeats silently. At the end of the counting trial they reported the number of counted heartbeats only verbally. We also asked them not to count their pulse or attempt to use other manipulations during heartbeat counting. The beginning and the end of the counting intervals were signaled acoustically. IS was estimated as the averaged over N trials heartbeat perception score:

$$IS = \frac{1}{N} \sum_{k=1}^{N} \left(1 - \frac{\left| N_k^{(r)} - N_k^{(c)} \right|}{N_k^{(r)}} \right), \tag{E.1}$$

where $N_k^{(c)}$ and $N_k^{(r)}$ are the numbers of the counted and actually recorded heartbeats within the k-th trial.

Time estimation error scores were analysed using a repeated-measures analysis of variance (ANCOVA) with the factors Interval Length (eight levels) and IS as covariate.

We also computed the heart rate variability (HRV). For this goal we first obtained all normal interbeat intervals $RR_k = t_{k+1} - t_k$ and then computed their average, the standard deviation, and the root mean square of the successive differences (RMSSD). The RMSSD, an indicator of vagal activity, is derived from the HRV as

$$RMSSD = \sqrt{\frac{1}{M-1} \sum_{k=1}^{M-1} (RR_{k+1} - RR_k)^2},$$

where M is the number of RR intervals. Then, we performed a correlation analysis of IS, synchronization indices, and HRV measures.

E.2. Results

We calculated the correlation between vagal cardiac control (RMSSD) and IS. The correlation coefficient obtained was significantly positive with $r = 0.48$ and statistically significance value (p-value) $p < 0.05$. This indicated that IS is associated with greater vagal control of the heart.

Next, we assessed the correlation between time perception accuracy (mean score across all time intervals) and vagal cardiac control (RMSSD). We obtained a significant negative correlation coefficient of $r = -0.34$ ($p < .05$). This result means that a higher RMSSD is associated with lower time estimation error, i.e. a better time reproduction accuracy.

Finally, we carried out correlation analysis to check whether higher synchronization is associated with time reproduction accuracy or with IS. We found significant correlation between IS and synchronization index (SI) (see section 4.3) only for 2 seconds time interval. The result is shown in Fig. E.1.
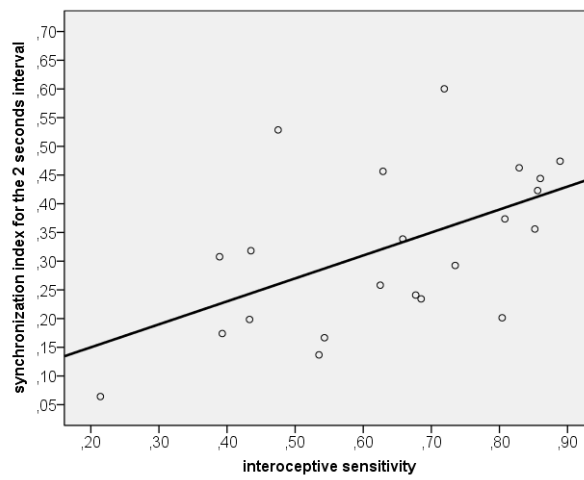
Figure E.1.: Scatterplot between interoceptive sensitivity and the maximum synchronization index for the 2s time interval. Positive correlation coefficient $r = 0.54$ with statistically significance value (p-value) $p < 0.05$ indicates that participants with higher IS show higher degree of synchronization between heart cycle and time reproduction begin/end responses. From [59].

Bibliography

[1] D. M. Abrams, R. Mirollo, S. H. Strogatz, and D. A. Wiley. Solvable model for chimera states of coupled oscillators. *Phys. Rev. Lett.*, 101:084103, 2008.

[2] D. M. Abrams and S. H. Strogatz. Chimera states for coupled oscillators. *Phys. Rev. Lett.*, 93(17):174102, 2004.

[3] L. Astolfi, F. De Vico Fallani, F. Cincotti, D. Mattia, M. G. Marciani, S. Salinari, J. Sweeney, G. A. Miller, B. He, and F. Babiloni. Estimation of effective and functional cortical connectivity from neuroelectric and hemodynamic recordings. *IEEE transactions on neural systems and rehabilitation engineering : a publication of the IEEE Engineering in Medicine and Biology Society*, 17(3):224–33, June 2009.

[4] P. Barbara, A. B. Cawthorne, S. V. Shitov, and C. J. Lobb. Stimulated emission and amplification in josephson junction arrays. *Phys. Rev. Lett.*, 82:1963–1966, Mar 1999.

[5] D. Battogtokh and Y. Kuramoto. Turbulence of nonlocally coupled oscillators in the benjamin-feir stable regime. *Phys. Rev. E*, 61:3227–3229, Mar 2000.

[6] Jerry J Batzel and Franz Kappel. Time delay in physiological systems: analyzing and modeling its impact. *Mathematical biosciences*, 234(2):61–74, December 2011.

[7] J.J. Batzel and F. Kappel. Time delay in physiological systems: analyzing and modeling its impact. *Math Biosci.*, 234(2):61–74, 2011.

[8] Richard A. Block, Peter A. Hancock, and Dan Zakay. How cognitive load affects duration judgments: A meta-analytic review. *Acta psychologica*, 134(3):330–43, July 2010.

[9] Grigory Bordyugov, Arkady Pikovsky, and Michael Rosenblum. Self-emerging and turbulent chimeras in oscillator chains. *Phys. Rev. E*, 82(3):035205, Sep 2010.

[10] W. Braun, A. Pikovsky, M. A. Matias, and P. Colet. Global dynamics of oscillator populations under common noise. *EPL*, 99:20006, 2012.

[11] Maja Lotrič Bračič and Aneta Stefanovska. Synchronization and modulation in the human cardiorespiratory system. *Physica A: Statistical Mechanics and its Applications*, 283(3-4):451–461, August 2000.

[12] M. Breakspear, S. Heitmann, and A. Daffertshofer. Generative models of cortical oscillations: neurobiological implications of the Kuramoto model. *Front. Human Neurosci.*, 4:190, 2010.

[13] R. M. Corless, G. H. Gonnet, D. E. G. Hare, D. J. Jeffrey, and D. E. Knuth. On the LambertW function. *Advances in Computational Mathematics*, 5(1):329–359, December 1996.

[14] A. D. Bud Craig. Emotional moments across time: a possible neural basis for time perception in the anterior insula. *Philosophical transactions of the Royal Society of London. Series B, Biological sciences*, 364(1525):1933–42, July 2009.

[15] A. D. Bud Craig. How do you feel–now? The anterior insula and human awareness. *Nature reviews. Neuroscience*, 10(1):59–70, January 2009.

[16] Hugo D. Critchley, Stefan Wiens, Pia Rotshtein, Arne Ohman, and Raymond J. Dolan. Neural systems supporting interoceptive awareness. *Nature neuroscience*, 7(2):189–95, February 2004.

[17] H. Daido and K. Nakanishi. Diffusion-induced inhomogeneity in globally coupled oscillators: Swing-by mechanism. *Phys. Rev. Lett.*, 96:054101, 2006.

[18] A. R. Damasio. *Descartes' Error: Emotion, Reason and the Human Brain.* Grosset/Putman, New York, NY, 1994.

[19] Z. Dombovari, R. E. Wilson, and G. Stepan. Estimates of the bistable region in metal cutting. *Proceedings of the Royal Society A: Mathematical, Physical and Engineering Sciences*, 464(2100):3255–3271, December 2008.

[20] Giovanni Filatrella, Niels Falsig Pedersen, and Kurt Wiesenfeld. High-q cavity-induced synchronization in oscillator arrays. *Phys. Rev. E*, 61:2513–2518, Mar 2000.

[21] Giovanni Giacomelli, Francesco Marino, Michael a. Zaks, and Serhiy Yanchuk. Coarsening in a bistable system with long-delayed feedback. *EPL (Europhysics Letters)*, 99(5):58005, September 2012.

[22] L. Glass. Synchronization and rhythmic processes in physiology. *Nature*, 410(6825):277–84, March 2001.

[23] L. Glass and M. C. Mackey. *From Clocks to Chaos: The Rhythms of Life.* Princeton Univ. Press, Princeton, NJ, 1988.

[24] D. Goldobin, M. Rosenblum, and A. Pikovsky. Controlling oscillator coherence by delayed feedback. *Phys. Rev. E*, 67(6):061119, 2003.

[25] D. Golomb, D. Hansel, and G. Mato. Mechanisms of synchrony of neural activity in large networks. In F. Moss and S. Gielen, editors, *Neuro-informatics and Neural Modeling*, volume 4 of *Handbook of Biological Physics*, pages 887–968. Elsevier, Amsterdam, 2001.

[26] N. D. Hayes. Roots of the Transcendental Equation Associated with a Certain Difference-Differential Equation. *Journal of the London Mathematical Society*, s1-25(3):226–232, July 1950.

[27] Tamás Insperger and Gábor Stépán. *Semi-Discretization for Time-Delay Systems*, volume 178 of *Applied Mathematical Sciences*. Springer New York, New York, NY, 2011.

[28] M. Iwanaga. Harmonic relationship between preferred tempi and heart rate. *Perceptual and motor skills*, 81(1):67–71, August 1995.

[29] Williams James. What is an emotion? *Mind*, os-IX(34):188–205, 1884.

[30] G. E. Jones. Perception of visceral sensations: a review of recent findings, methodologies, and future directions. In J. R. Jenning and P. K. Ackles, editors, *Advances in Psychophysiology Vol.5*, pages 155–192. Jessica Kingsley Publishers, London, 1994.

[31] K. Kaneko. Clustering, coding, switching, hierarchical ordering, and control in a network of chaotic elements. *Physica D*, 41:137–172, 1990.

[32] R. Kapral and K. Showalter. *Chemical waves and Patterns.* Kluwer, Dordrecht, 1995.

[33] Y. Kuramoto. Self-entrainment of a population of coupled nonlinear oscillators. In H. Araki, editor, *International Symposium on Mathematical Problems in Theoretical Physics*, page 420, New York, 1975. Springer Lecture Notes Phys., v. 39.

[34] Y. Kuramoto. *Chemical Oscillations, Waves and Turbulence.* Springer, Berlin, 1984.

[35] Y. Kuramoto and D. Battogtokh. Coexistence of coherence and incoherence in nonlocally coupled phase oscillators. *Nonlinear Phenom. Complex Syst.*, 5:380–385, 2002.

[36] Carlo R. Laing. The dynamics of chimera states in heterogeneous kuramoto networks. *Physica D: Nonlinear Phenomena*, 238(16):1569 – 1588, 2009.

[37] Carlo R. Laing, Karthikeyan Rajendran, and Ioannis G. Kevrekidis. Chimeras in random non-complete networks of phase oscillators. *Chaos: An Interdisciplinary Journal of Nonlinear Science*, 22(1):–, 2012.

[38] Lambert J.H. Observationes variae in mathesin puram. *Acta Helveticae physico-mathematico-anatomico-botanico-medica*, (Band III):128–168, 1758.

[39] Seung-Hwan Lee, Young-Min Park, Do-Won Kim, and Chang-Hwan Im. Global synchronization index as a biological correlate of cognitive decline in Alzheimer's disease. *Neuroscience research*, 66(4):333–9, April 2010.

[40] E. A. Martens, S. Thutupalli, A. Fourriere, and O. Hallatschek. Chimera states in

mechanical oscillator networks. *Proceedings of the National Academy of Sciences*, pages 1–5, June 2013.

[41] Erik A. Martens, Carlo R. Laing, and Steven H. Strogatz. Solvable model of spiral wave chimeras. *Phys. Rev. Lett.*, 104:044101, Jan 2010.

[42] C. Masoller. Noise-induced resonance in delayed feedback systems. *Phys. Rev. Lett.*, 88(3):034102, 2002.

[43] William Mather, Matthew Bennett, Jeff Hasty, and Lev Tsimring. Delay-Induced Degrade-and-Fire Oscillations in Small Genetic Circuits. *Physical Review Letters*, 102(6):068105, February 2009.

[44] A. McRobie, G. Morgenthal, J. Lasenby, and M. Ringer. *Proc. Inst. Civ. Eng. Bridge Eng.*, 156:71–79, 2003.

[45] Karin Meissner and Marc Wittmann. Body signals, cardiac awareness, and the perception of time. *Biological psychology*, 86(3):289–97, March 2011.

[46] P.K. Mohanty and A. Politi. A new approach to partial synchronization in globally coupled rotators. *J. Phys. A: Math. Gen.*, 39(26):L415–L421, 2006.

[47] R. Y. Moore. CIRCADIAN RHYTHMS:A Clock for the Ages. *Science*, 284(5423):2102–2103, June 1999.

[48] Florian Mormann, Klaus Lehnertz, Peter David, and Christian E. Elger. Mean phase coherence as a measure for phase synchronization and its application to the EEG of epilepsy patients. *Physica D: Nonlinear Phenomena*, 144(3-4):358–369, October 2000.

[49] Ralf Mrowka, Andreas Patyzk, and M. Rosenblum. Qualitative analysis of cardiorespiratory synchronization in infants. *International Journal of Bifurcation and Chaos*, 10(11):2479–2488, November 2000.

[50] E. Niebur, H. G. Schuster, and D. M. Kammen. Collective frequencies and metastability in networks of limit-cycle oscillators with time delay. *Phys. Rev. Lett.*, 67(20):2753–2756, 1991.

[51] Simbarashe Nkomo, Mark R. Tinsley, and Kenneth Showalter. Chimera states in populations of nonlocally coupled chemical oscillators. *Phys. Rev. Lett.*, 110:244102, Jun 2013.

[52] Oleh E. Omelchenko, Yuri L. Maistrenko, and Peter A. Tass. Chimera states: The natural link between coherence and incoherence. *Phys. Rev. Lett.*, 100:044105, Jan 2008.

[53] Mark J. Panaggio and Daniel M. Abrams. Chimera states on a flat torus. *Phys. Rev. Lett.*, 110:094102, Feb 2013.

[54] A. Pikovsky and M. Rosenblum. Partially integrable dynamics of hierarchical populations of coupled oscillators. *Phys. Rev. Lett.*, 101:264103, 2008.

[55] A. Pikovsky, M. Rosenblum, and J. Kurths. *Synchronization. A Universal Concept in Nonlinear Sciences.* Cambridge University Press, Cambridge, 2001.

[56] Olga Pollatos, Klaus Gramann, and Rainer Schandry. Neural systems connecting interoceptive awareness and feelings. *Human brain mapping*, 28(1):9–18, January 2007.

[57] Olga Pollatos, Beate M. Herbert, Christian Kaufmann, Dorothee P. Auer, and Rainer Schandry. Interoceptive awareness, anxiety and cardiovascular reactivity to isometric exercise. *International journal of psychophysiology : official journal of the International Organization of Psychophysiology*, 65(2):167–73, August 2007.

[58] Olga Pollatos, Wladimir Kirsch, and Rainer Schandry. On the relationship between interoceptive awareness, emotional experience, and brain processes. *Brain research. Cognitive brain research*, 25(3):948–62, December 2005.

[59] Olga Pollatos, Azamat Yeldesbay, Arkady Pikovsky, and Michael Rosenblum. How much time has passed? Ask your heart. *Frontiers in neurorobotics*, 8:15, January 2014.

[60] E. Rodriguez, N. George, J. P. Lachaux, J. Martinerie, B. Renault, and F. J. Varela. Perception's shadow: long-distance synchronization of human brain activity. *Nature*, 397(6718):430–3, February 1999.

[61] M. Rosenblum and A. Pikovsky. Self-organized quasiperiodicity in oscillator ensembles with global nonlinear coupling. *Phys. Rev. Lett.*, 98:064101, 2007.

[62] H. Sakaguchi and Y. Kuramoto. A soluble active rotator model showing phase transition via mutual entrainment. *Prog. Theor. Phys.*, 76(3):576–581, 1986.

[63] Carsten Schäfer, Michael Rosenblum, Hans-Henning Abel, and Jürgen Kurths. Synchronization in the human cardiorespiratory system. *Physical Review E*, 60(1):857–870, July 1999.

[64] L. Schmidt, K. Schönleber, K. Krischer, and V. García-Morales. Coexistence of synchrony and incoherence in oscillatory media under nonlinear global coupling. *Chaos*, 24(1):013102, 2014.

[65] Gautam C. Sethia and Abhijit Sen. Chimera States: The Existence Criteria Revisited. *Physical Review Letters*, 112(14):144101, April 2014.

[66] Gautam C. Sethia, Abhijit Sen, and Fatihcan M. Atay. Clustered chimera states in delay-coupled oscillator systems. *Phys. Rev. Lett.*, 100:144102, Apr 2008.

[67] Hiroshi Shinozaki and Takehiro Mori. Robust stability analysis of linear time-delay systems by Lambert function: Some extreme point results. *Automatica*, 42(10):1791–1799, October 2006.

[68] Gabor Stepan. *Retarded dynamical systems: Stability and characteristic functions*. Longman, London, 1989.

[69] Jesse Stricker, Scott Cookson, Matthew R Bennett, William H Mather, Lev S Tsimring, and Jeff Hasty. A fast, robust and tunable synthetic gene oscillator. *Nature*, 456(7221):516–9, November 2008.

[70] S. H. Strogatz, D. M. Abrams, A. McRobie, B. Eckhardt, and E. Ott. Theoretical mechanics: Crowd synchrony on the Millennium Bridge. *Nature*, 438:43–44, 2005.

[71] S.H. Strogatz. *Sync: How Order Emerges From Chaos In the Universe, Nature, and Daily Life.* Hyperion, 2003.

[72] a Takamatsu, T Fujii, and I Endo. Time delay effect in a living coupled oscillator system with the plasmodium of Physarum polycephalum. *Physical review letters*, 85(9):2026–9, August 2000.

[73] P. Tass, M. G. Rosenblum, J. Weule, J. Kurths, A. Pikovsky, J. Volkmann, A. Schnitzler, and H.-J. Freund. Detection of n:m Phase Locking from Noisy Data: Application to Magnetoencephalography. *Physical Review Letters*, 81(15):3291–3294, October 1998.

[74] M. R. Tinsley, S. Nkomo, and K. Showalter. Chimera and phase-cluster states in populations of coupled chemical oscillators. *Nature Physics*, 8(9):662–665, July 2012.

[75] Michel Treisman, Norman Cook, Peter L. N. Naish, and Janice K. MacCrone. The internal clock: Electroencephalographic evidence for oscillatory processes underlying time perception. *The Quarterly Journal of Experimental Psychology Section A*, 47(2):241–289, May 1994.

[76] C. van Vreeswijk. Partial synchronization in populations of pulse-coupled oscillators. *Phys. Rev. E*, 54(5):5522–5537, 1996.

[77] Stefan Wiens. Interoception in emotional experience. *Current Opinion in Neurology*, 18(4):442–447, August 2005.

[78] A. Wilmer, M. H. E. de Lussanet, and M. Lappe. A method for the estimation of functional brain connectivity from time-series data. *Cognitive neurodynamics*, 4(2):133–49, June 2010.

[79] A. T. Winfree. Biological rhythms and the behavior of populations of coupled oscillators. *J. Theor. Biol.*, 16:15–42, 1967.

[80] A. T. Winfree. *The Geometry of Biological Time.* Springer, Berlin, 1980.

[81] Marc Wittmann. The inner experience of time. *Philosophical transactions of the Royal Society of London. Series B, Biological sciences*, 364(1525):1955–67, July 2009.

[82] Marc Wittmann, Alan N Simmons, Taru Flagan, Scott D Lane, Jiří Wackermann, and Martin P Paulus. Neural substrates of time perception and impulsivity. *Brain research*, 1406:43–58, August 2011.

[83] M. Wolfrum, O. E. OmelâĂŹchenko, S. Yanchuk, and Y. L. Maistrenko. Spectral properties of chimera states. *Chaos: An Interdisciplinary Journal of Nonlinear Science*, 21(1):–, 2011.

[84] Azamat Yeldesbay, Arkady Pikovsky, and Michael Rosenblum. Chimeralike States in an Ensemble of Globally Coupled Oscillators. *Physical Review Letters*, 112(14):144103, April 2014.

[85] Y. Zhu, Y. Li, M. Zhang, and J. Yang. The oscillating two-cluster chimera state in non-locally coupled phase oscillators. *EPL (Europhysics Letters)*, 97(1):10009, 2012.